Materials & Design 206 (2021) 109750

Contents lists available at ScienceDirect

Materials & Design

journal homepage: www.elsevier.com/locate/matdes

A new route for developing ultrafine-grained Al alloy strips using repetitive bending under tension

Saeed Tamimi [a,*], Giribaskar Sivaswamy [a], Hadi Pirgazi [b], Babak Shalchi Amirkhiz [c], Shanmukha Moturu [a], M. Amir Siddiq [d], Winfried Kockelmann [e], Paul Blackwell [a,f]

[a] Advanced Forming Research Centre (AFRC), University of Strathclyde, Glasgow, United Kingdom
[b] Department of Electromechanical, Systems and Metal Engineering, Ghent University, Ghent, Belgium
[c] CanmetMATERIALS of Natural Resources Canada, Hamilton, ON, Canada
[d] School of Engineering, University of Aberdeen, Aberdeen, United Kingdom
[e] Rutherford Appleton Laboratory, Science and Technology Facilities Council (STFC), ISIS Facility, Harwell, United Kingdom
[f] Department of Design, Manufacturing and Engineering Management, University of Strathclyde, Glasgow, United Kingdom

ARTICLE INFO

Article history:
Received 26 January 2021
Revised 11 April 2021
Accepted 15 April 2021
Available online 20 April 2021

Keywords:
Repetitive bending under tension
Severe plastic deformation
AA-7075 strip
Grain refinement

ABSTRACT

In this work, the mechanical behaviour and microstructure changes of AA-7075 alloy subjected to a repetitive-bending-under-tension (R-BUT) process were studied. In the R-BUT process, a metallic strip undergoes repeated localised bending and unbending. Load-displacement curves derived from R-BUT tested samples displayed a drastic increase in elongation to failure as compared to samples subjected to standard tensile tests. Additionally, the results confirmed that the force required to deform the R-BUT samples is much reduced as compared to the load required during simple tension. Finite element analysis confirmed that the sample subjected to the R-BUT process underwent intense shear deformation. Transmission-electron-microscopy (TEM) and electron-backscattered-diffraction (EBSD) analysis of the deformed matrix from the ND-RD plane (through-thickness) exhibited evidence for the formation of fine grains. TEM analysis confirmed that the fine grains formed were in the size range of 200–400 nm. Intense shear deformation experienced by the matrix led to shearing followed by spheroidization of precipitate particles. The influence of precipitate particles on the grain refinement process through Particle Stimulated Nucleation of fine grains in the matrix is also presented. EBSD analysis suggested that a Continuous Dynamic Recrystallisation process is the key mechanism behind the grain refinement in the sample during R-BUT processing.

1. Introduction

Thriving human populations, globalisation and global warming have made both the manufacturing sector and consumers focus on technologies to produce products which can be recyclable, reduce carbon emission, be cost-effective and flexible to accommodate future demands. Severe plastic deformation (SPD) is a technology that can be used in aerospace and the bio-medical industries for producing bulk ultrafine-grained materials without compromising component dimensional tolerance [1]. There are a range of processes that are classified as inducing severe plastic deformation, these include equal channel angular pressing (ECAP) [2,3], incremental equal channel angular pressing (I-ECAP) [4,5], high pressure torsion (HPT) [6,7], accumulative roll bonding (ARB) [8,9], multi axial forging (MAF) [10,11], repetitive corrugation and straightening (RCS) [12,13], twist extrusion (TE) [14,15] and constrained groove pressing (CGP) [16,17]. Some of these are used primarily for research, others to produce low volume components. Among them, ARB, RCS and CGP are primarily techniques that have been used to fabricate ultrafine-grained (UFG) sheet materials. In all SPD operations, shear plastic deformation applied through the process is a crucial factor in grain refinement. Lee et al. calculated the shear straining introduced by different passes of ARB and correlated this to the grain size distribution through the Al sheet thickness [18]. It has also been shown how shear straining distributed through the sheet thickness in the different cycles of RCS changes the microstructure of aluminium sheet [19]. Kumar et al. explained how the bending and unbending through flattening occurring in CGP can introduce shear plastic deformation in each pass. In the following CGP cycle this shear straining increases and impacts on the microstructure of the aluminium sheets [16].

* Corresponding author.
E-mail address: saeed.tamimi@strath.ac.uk (S. Tamimi).

https://doi.org/10.1016/j.matdes.2021.109750
0264-1275/

Basically, in both the SPD processes of CGP and RCS, repetitive bending and unbending has significant impact on microstructure and, depending on the number of passes, it can reduce the grain size below 1 μm. Repetitive Bending under Tension (R-BUT) could be a promising new manufacturing operation capable of fabricating UFG materials. R-BUT is a testing methodology equipped with three sliding rollers configured similar to the three-point bending test (see Fig. 1). The three rollers slide up and down in cycles along the gauge volume to bend and unbend the sample, at the same time pulling the specimen in tension. In this process necking localization is postponed, and material can be deformed far beyond its standard elongation in simple tension [20]. The bending and unbending in a repetitive manner occurring during the process can play a crucial role in grain refinement, similar to that occurring in bending/unbending type SPD operations e.g. CGP, RCS and CGR. However, the larger bending radius and a significant higher number of cycles achievable in R-BUT compared to other SPD operations can have a more effective impact on grain refinement. Originally, Benedyk et al. in 1971, introduced R-BUT to study the high strain deformation of materials as observed in some incremental forming or forging operations, in particular in the automotive industry [21]. Emmens et al. performed R-BUT experiments to understand the impact of test parameters like speed and bending levels on material elongation [22]. They concluded that the pulling speed and depth setting are key parameters for achieving enhanced elongation properties of materials. Moreover, it was shown that formability of the material is reduced when roller speed is low due to an increase in the number of bending and unbending cycles. Roemer et al. [23] and Barrett et al. [24] demonstrated that Al-6022-T4 sheet material is twice as ductile in the R-BUT test in comparison to a tensile test. Zecevic et al. [25] and Poulin et al. [26] have reported a strong (1 1 1) fibre texture in Al6022-T4, and (0 1 1) fibre texture in dual phase steels for R-BUT tested samples. In recent work by the authors, the favourable impact of R-BUT on the mechanical behaviour of commercially pure titanium has been reported and possible reasons for the observed enhancement in elongations have been discussed [20]. Although there are a number of research works focusing on enhancing mechanical properties of materials through R-BUT, there is no investigation or feasibility study of this manufacturing operation for fabricating UFG materials. Therefore, this study aims at evaluating the capability of the R-BUT process in making UFG AA-7075 sheets at room temperature.

2. Experimental procedure

2.1. Material

In this study, AA7075 aluminium alloy in the form of sheet metal having thicknesses around 2 mm and 3 mm are selected. The chemical analysis of this alloy is given in Table 1.

2.2. R-BUT testing

The test rig used for performing the R-BUT operation was developed at the University of Strathclyde. The R-BUT testing rig was attached to a Zwick/Roell Z150 standard mechanical testing

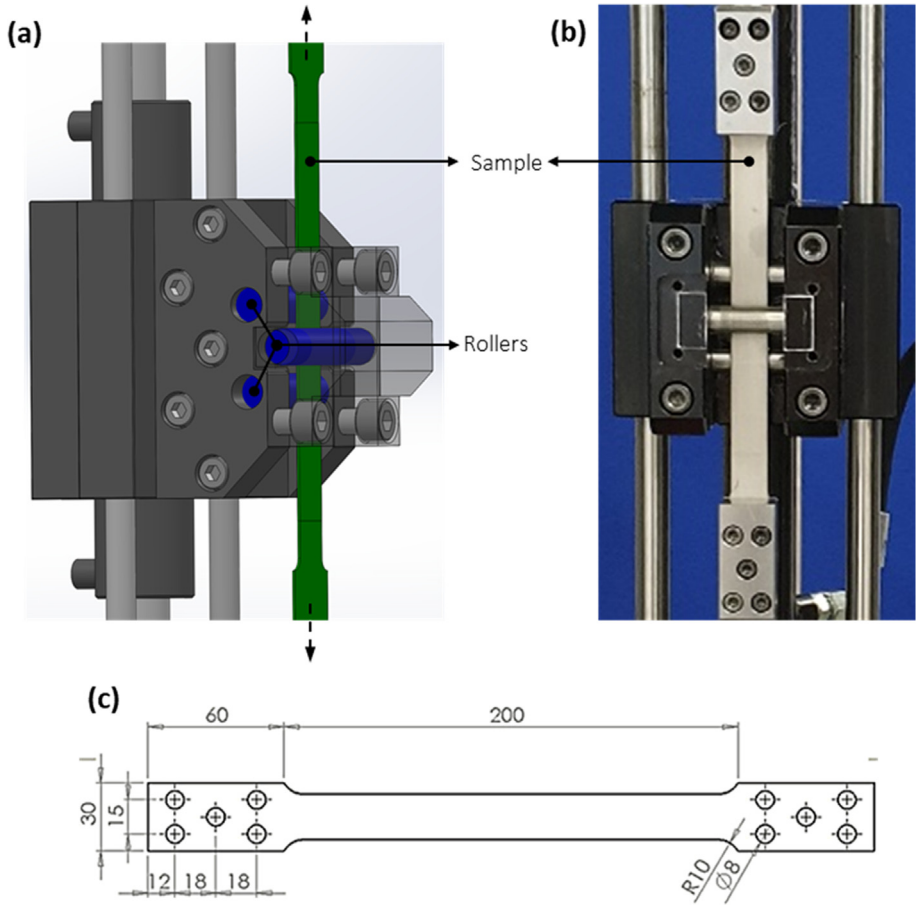

Fig. 1. (a) CAD model of the R-BUT assembly, (b) a photograph illustrating the actual testing rig attached to a Zwick/Roell Z150 testing machine and (c) R-BUT testing sample. All dimensions are in mm.

Table 1
Nominal chemical composition of AA-7075 alloy (wt.%).

Zn	Mg	Cu	Al
5.6	2.5	1.6	Balance

Table 2
R-BUT test matrix.

	Tensile test	Set 1	Set 2	Set 3	Set 4
Penetration Depth (mm)	0	1	2	4	2
ω	N/A	200	200	200	800

machine. A CAD model and a photograph of the test rig is shown in Fig. 1. The R-BUT testing rig consists of three 35 mm diameter rollers which apply 3-point bending on the sheet metal sample selected for testing. The bending assembly slides along the sample with controllable/adjustable velocities. Further technical details of the R-BUT testing rig have been reported in a previous study [20]. Briefly, setting up the R-BUT testing includes the following steps:

1. Clamping the sample;
2. Applying bending using an adjustable roller;
3. Applying a pulling load where simultaneously the roller assembly starts moving up and down with a controlled velocity.

A number of trials were performed to study the influence of the major experimental parameters associated with the R-BUT test. The prominent R-BUT parameters include the bending levels, the travel velocity of the bending assembly and the pulling velocity applied along the length of the strip. Since the straining condition can be controlled by both the pulling velocity and the bending assembly velocity, the term ω is defined as the ratio of bending and pulling velocities as shown in Eq. (1):

$$\omega = \frac{bending\ \ assembly\ \ velocity\ \ (mm/s)}{pulling\ \ velocity\ \ (mm/s)} \tag{1}$$

A three point bending condition can be achieved by penetration of the adjustable roller towards the other rollers. Therefore, any increase in penetration depth will lead to an increase in the bending levels which in turn decreases the bending radius. Table 2 presents the selected test matrix in this study. As elaborated, the two main parameters of the bending penetration as well as ω have been targeted. All experiments were conducted at room temperature and under a fully lubricated condition to minimize the friction due to roller contact effects and also to avoid any surface damage. The sample geometry adopted for R-BUT tests is given in Fig. 1(c) and the samples for this work were extracted using waterjet cutting from a blank of AA-7075 alloy.

2.3. Finite element modelling of the R-BUT process

The finite element model of the R-BUT process was constructed based on the experimental test setup described in Section 2.2. The testing sample was modelled using 10,815 three-dimensional reduced integration Hexagonal (C3D8R) elements. The size of elements was selected after performing mesh sensitivity analysis. Since the rollers used in the experiments were much stiffer than the testing samples, these were modelled using 3239 three dimensional rigid elements (RNODE3D) to reduce computational time. Interaction between the rollers and sample was defined using a general contact algorithm in ABAQUS; this formulation automatically detects the contact once established. All exterior surfaces were included in the analysis for active contact checking. The contact pressure between the contacting surfaces was computed using the hard contact formulation available in ABAQUS. This formulation computes the contact pressure based on the applied loading and material stiffness. As shown in Fig. 2, the analyses comprised of two explicit dynamic steps, i.e. an initial penetration step where one of the rollers penetrated in the horizontal direction while keeping the rest of the rollers and both (top and bottom) surfaces of the samples fixed in the horizontal and vertical directions (middle figure). Penetrations of 2 and 4 mm were used in the present study. For step 2, the roller positions were locked in the horizontal plane and movement in the vertical plane was simulated simultaneously with tensile deformation as shown in Fig. 2 (right; step 2). The roller speed used for these analyses was 40 mm/sec. To achieve this, each roller is constrained at its centre to restrict its linear motion along the horizontal axis while also restricting rotations about the horizontal and vertical axes. A velocity boundary condition was applied, to simulate roller motion, using an amplitude function to translate the rollers in the vertical direction (Fig. 2 right). Results of the simulations are discussed in Section 3.1.

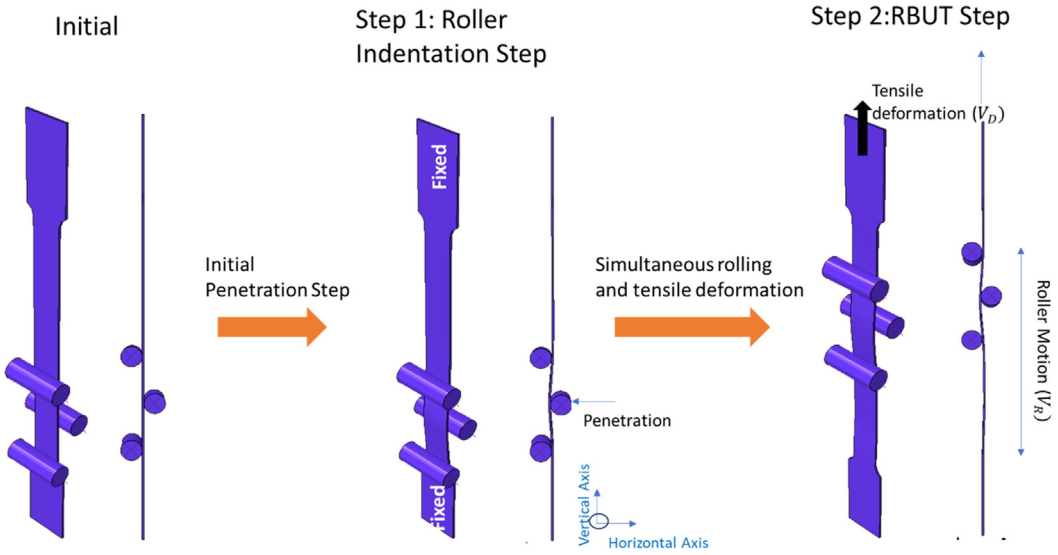

Fig. 2. Finite element setup illustrating the steps considered for FE modelling sample subjected to R-BUT process.

2.4. Microstructural characterisation

2.4.1. TEM analysis

For TEM observations, the coupons from the tensile and R-BUT tested samples were sectioned using a slow speed diamond saw to cut slices of thicknesses around 400 μm. These slices were mechanically polished to decrease the thickness to 80–100 μm. Discs of 3 mm diameter were punched out using Gatan punch (Model 659). The final polishing was done by using a twin-jet electro-polisher with A2 electrolyte, at 15 V and 40 mA. The temperature of the electrolyte bath used for the twin jet electro-polishing was maintained in the range −25 °C to −30 °C. A Struers Tenupol5 twin jet polisher was used to thin the centre of the thin foils until perforation, without introducing artifacts, so that the areas around the hole were electron transparent. Ethanol was used for final cleaning of the twin-jet polished samples. TEM observations were made using a FEI Tecnai Osiris TEM microscope operating at 200 kV (X-FEG gun). The imaging modes in this work were bright field (BF) and dark field (DF). Selected area diffraction patterns (SADP) were recorded to assess the degree of grain refinement. Moreover, electron X-ray energy dispersive spectroscopy (EDS) was conducted in the scanning mode (STEM) to acquire chemical data including elemental mapping. Samples for microstructural analysis were extracted from coupons cut out close to the fracture tip from the ND-RD plane.

2.4.2. EBSD analysis

The microstructural characteristics of the as-received and processed samples were analysed using the Electron Back Scattering Diffraction (EBSD) technique. Samples from the ND-RD plane were used for this analysis. The EBSD scans were carried out in a FEI Quanta™ 450 FEG-SEM microscope over an area with a dimension of 1,200 × 1,000 μm^2 using a step size of 1.5 μm for all the scans. Furthermore, higher magnification EBSD scans (60 × 60 μm^2 with a step size of 100 nm) were collected to analyse the deformation characteristics of aluminium matrix after R-BUT. TSL® OIM data collection software was used for completing the EBSD scans and also for post processing. EBSD datasets were subjected to a two-step clean-up procedure, i.e. neighbour orientation correlation (grain tolerance angle 5°, minimum confidence index 0.1 and 5th level neighbour orientation correlation) and grain dilation correction (grain tolerance angle of 5° and a minimum grain size of 4 pixels) using the OIM analysis software.

2.4.3. Bulk texture analysis

The texture of the R-BUT samples was analysed using the General Materials Diffractometer (GEM) instrument at ISIS neutron facilities in Oxford [27]. The advantage of the neutron diffraction over other diffraction techniques is that it offers a higher penetration depth, bulk and local texture analysis, no sample preparation was required, no sample rotation is required and a complete pole figure is obtained in a short time due to the time-of-flight analysis at the ISIS pulsed spallation neutron source. A range of neutron wavelengths between 0.2 and 3.5 Å was used for the measurements. The GEM instrument at ISIS is equipped with 7000 individual detector elements which for texture analysis are grouped into 164 banks, such that each bank covers approximately 10°×10° [27]. Three samples were allocated for bulk texture analysis in this study: (i) the as-received sample (ii) a uniaxial tensile sample and (iii) an R-BUT sample. In this study, a beam size of 20 × 10 mm^2 (height × width) was used to record in total 15 Bragg peaks at 20 min for each sample. In order to normalise the data to the wavelength distribution of the neutron flux and to convert the data into d spacing patterns, the Mantid software of the GEM instrument was used. Then, the Maud software [28] was employed to analyse the converted data using Rietveld fitting. The extended Williams Imhof Matthies Vinel (E-WIMV) algorithm in MAUD has been used for generating the normalised pole figures and Orientation Distribution Functions (ODF). The units for the normalised pole figure are expressed as multiples of a random distribution (m.r.d). Finally, the MTEX toolbox [29] was used to present the ODFs.

3. Results and discussion

3.1. Repetitive bending under tension of AA-7075

Before performing the R-BUT tests, room temperature tensile tests were conducted on samples of naturally aged AA-7075 sheets using the screw driven Zwick/Roell Z150 machine at an engineering strain rate of 10^{-3} s^{-1}. The engineering stress - engineering strain curve of the AA-7075 alloy derived from the load–displacement curves of samples from sheet of 2 mm thickness is presented in Fig. 3. The values of yield strength and ultimate tensile strength of this material are 98 and 215 MPa, respectively. The uniform elongation of the sample under uniaxial tension is 0.14. It is noted that the flow curve displayed serrations beyond the yield point during room temperature tensile testing. This heterogeneous plastic deformation is probably due to the Portevin-Le Chatelier (PLC) effect becoming activated under tensile loading. This could be associated with the interaction between solute atoms of Mg and the mobile dislocations, which is recognised as dynamic strain ageing [30]. In general, during plastic deformation, dislocations glide towards the loading direction using the available slip systems within the grains. During plastic deformation, dislocations form tangles which allows a cloud of solute atoms to condense around them. The driving force for this accumulation of solute atoms around the core of dislocations is to decrease the distortion in the crystal lattice. This is facilitated by pipe diffusion with mobile dislocations becoming trapped and pinned [31]. With the aid of stress, these solute atom clouds can be overcome by thermally activated dislocation motion. This dislocation-unpinning-process and also the long-range dislocation interactions, lead to a drop in the macroscopic stress value as can be seen in Fig. 3. It should be noted that the loading condition, as well as the microstructure state, can control the appearance of PLC effect in these materials i.e. the appearance of the PLC effect in these materials is influenced by presence of precipitates and test temperature, as well as strain rate.

Fig. 4 presents the load–displacement plots of the AA-7075 samples subjected to R-BUT with different penetration depths i.e. bending levels. For the sake of comparison, a load–displacement curve of a sample subjected to standard tensile testing with a same pulling rate of 0.2 mm/s is also presented in this figure. It is shown that the level of bending has a significant impact on the pulling force required to deform the sample. Higher bending levels lead to lower maximum forces taken by the specimen before fracture. During bending of the sample, a part of the cross section of the sheet is under tension and the other part of the cross section is under compression. These two sections are separated by neutral line, which is a function of the R-BUT parameters. It has been shown that the required pulling force to deform the sample under R-BUT depends on the area of cross-section which is under compressive straining [32]. For the sample with a higher penetration depth, more material in the cross section is under compression leading to a reduced force to deform the sample. It is noted that the bending deformation zone (the area in contact to the rollers) requires a lesser tensile force to deform the material plastically. This means that the rest of the material was under a lower force than the yield strength and therefore, remained within the elastic limit.

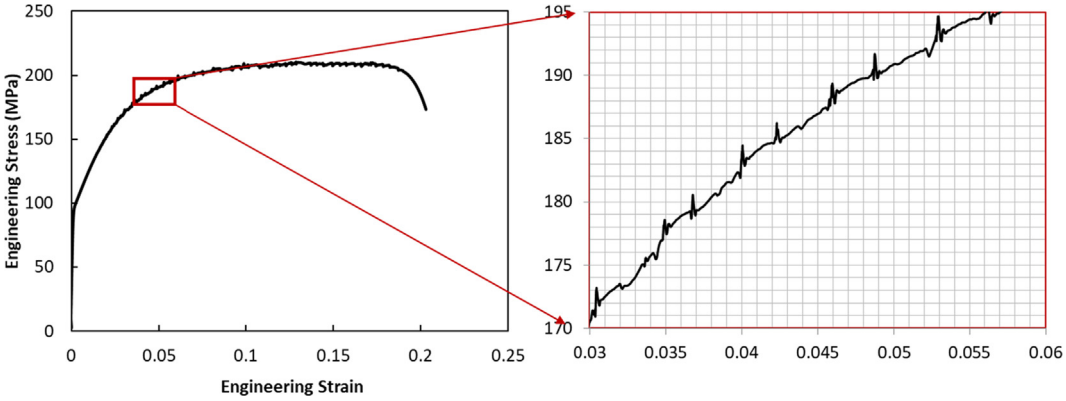

Fig. 3. Engineering stress - engineering strain curve of the as-received AA-7075 sheets under uniaxial tensile testing.

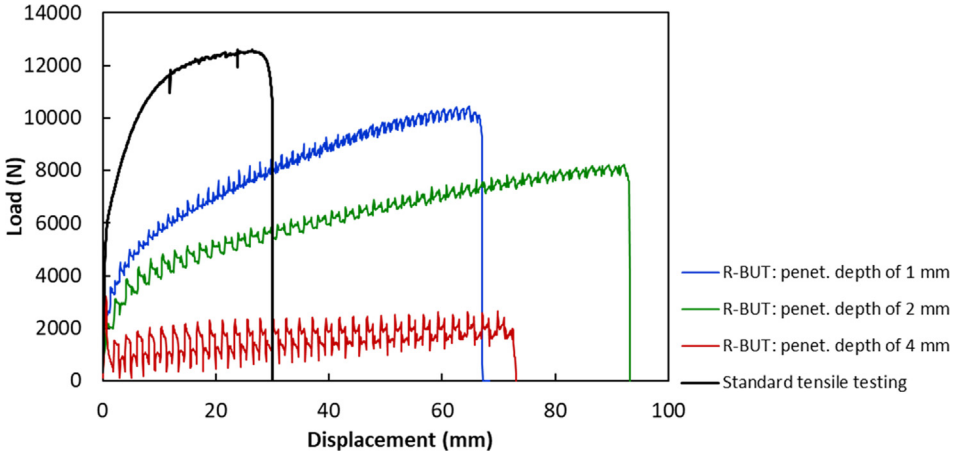

Fig. 4. Variation in load–displacement curves of AA-7075 alloy subjected to R-BUT under different bending levels.

Fig. 4 also shows that the samples subjected to R-BUT showed a higher level of displacement than their standard formability under tensile testing. A comparison among the R-BUT samples reveals that increasing the bending levels firstly leads to an increase and then a slight decrease in elongation as summarized in Table 3. In standard tensile testing, the sample fails as a result of initial 'diffuse necking' and rapid subsequent 'localised necking' after reaching the maximum tensile strength. This is marked by the formation of a deformation band at an angle of 54° to the first principal stress, i.e. the tensile direction. However, in the R-BUT process, the rollers change the local geometry and modify the stress state and localised necking is postponed. Furthermore, it has been previously reported that FE simulations have indicated that the sample under R-BUT conditions experiences a negative stress triaxiality resulting in late fracture compared to standard tensile testing where a positive stress triaxiality occurs [20].

The impact of the speed ratio, ω (EQUATION (1)), on the load–displacement curves of the aluminium sheets is presented in Fig. 5(a). Blue and red coloured curves indicate the R-BUT samples with ω = 200 and ω = 800, respectively. Penetration depth for both samples was the same at 2 mm. Although uniform formability and the maximum tensile force of the sample with ω = 200 is higher than the sample with ω = 800, the overall hardening rate for both cases was similar. Since the bending assembly speeds for these two cases were the same, the frequency of oscillation of bending and unbending for both cases equals 0.16 Hz at the beginning of the tests. It is however noticeable that the sample with ω = 200 failed after 42 cycles and the sample with ω = 800 failed after 158 cycles due to fracture. In the other words, each point of the sample with the blue curve, experienced 316 cycles of bending and unbending. The reason for this high number of R-BUT cycles of the samples with the higher ω could be associated with lower levels of tensile straining applied on the sample. Fig. 5(b) also presents the photograph of the sample which went up to fracture under R-BUT process with penetration depth of 2 mm and velocity ratio of 800.

Table 3
The effect of R-BUT with different bending levels on uniform elongations and maximum pulling forces.

Penetration depth (mm)	% Increase in fracture strain	% Decrease in maximum tensile force
0.0	reference	reference
1.0	126%	17%
2.0	226%	34%
4.0	142%	82%

Based on the FE models constructed in Section 2.3, analyses for different roller penetrations, tensile deformation speeds, and roller speeds, have been performed. Six of these results are presented here for brevity. Computational time for each simulation ranges from 9 days to 16 days depending on process parameters. Fig. 6 shows the plots of through thickness normalised plastic shear strain ratios to show the extent of plastic shear strains due to R-BUT. This normalised ratio is computed by dividing the plastic shear strains for the corresponding set of R-BUT process parameters with those from a conventional uniaxial test. The R-BUT process parameters varied are penetration depth, tensile deformation speed, and roller speed. It can be inferred from

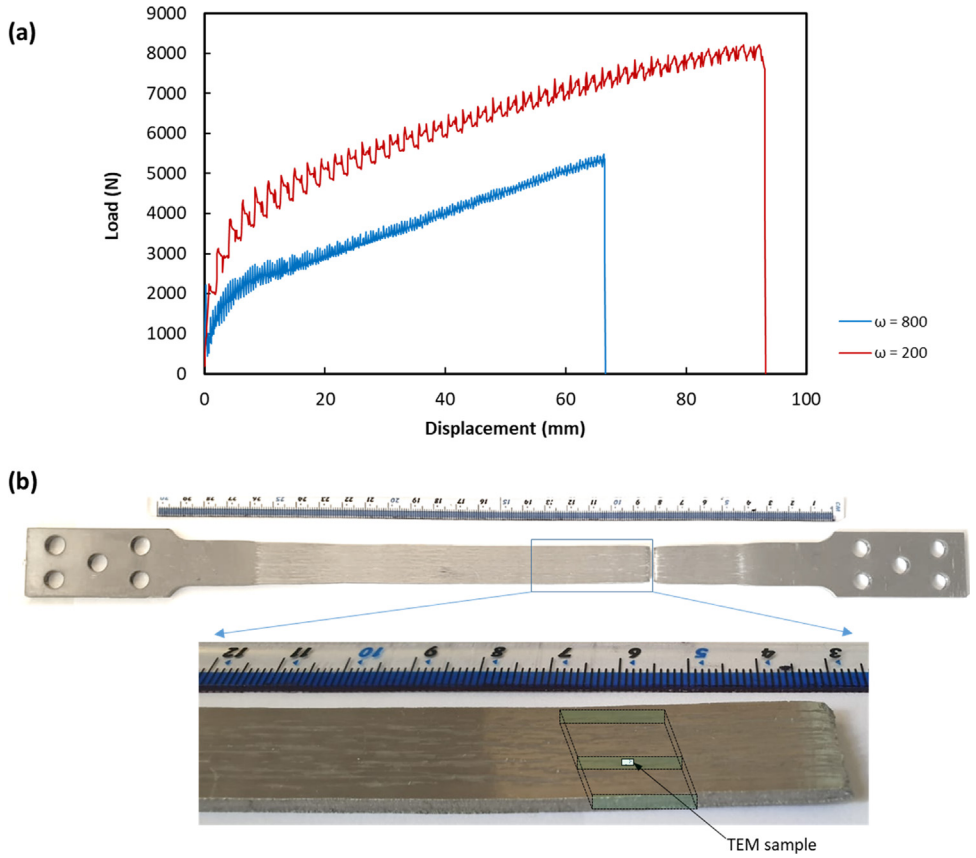

Fig. 5. (a) Variation in load–displacement curves of AA-7075 alloy subjected to R-BUT under different speed ratios; (b) photograph of an R-BUT processed sample and the location of through thickness TEM sample.

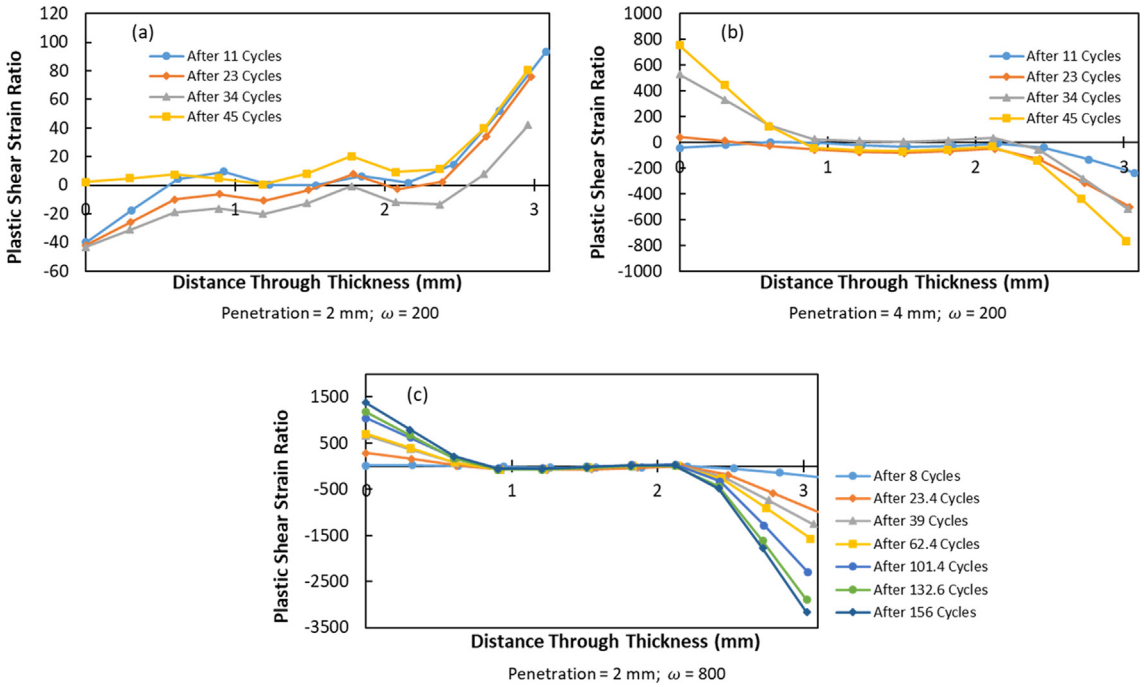

Fig. 6. (a-c) FE model predictions of the effect of R-BUT process parameters (penetration depth and velocity ratio,ω) on through thickness plastic shear strain ratio.

Fig. 6 that the plastic shear strain ratios are high near the surfaces while the central (middle) part of the sample is not significantly affected by the rollers. It was also found that increasing the penetration increases the plastic shear strain ratio throughout. The number of roller cycles had a significant effect on the plastic shear strains near the surfaces; as the number of roller cycles increased,

the plastic shear strains also increased. Additionally, it is noticeable that the plastic shear strains at the centre increase with an increasing number of cycles up to a point and then reverse directions. Tensile deformation speed increases the plastic shear strain ratios through the sample thickness for the same number of cycles.

Through thickness equivalent plastic strain ratios for the various R-BUT process parameters, such as penetration depth, tensile deformation speed, and roller speed are also plotted in Fig. 7. It was found that equivalent plastic strain ratios are high near the surfaces while central (middle) part of the sample was not significantly affected by the rollers. It can also be inferred from Fig. 7 that increasing the penetration depth increases the equivalent plastic strains throughout. The equivalent plastic strains near to the surfaces increased with an increasing number of cycles, whereas at the centre these strains saturated after a certain number of cycles which was dependent on penetration depth and deformation speed.

3.2. Microstructural characteristics

3.2.1. EBSD- microstructure and misorientation profiles

The normal direction inverse pole figure (ND-IPF) maps from EBSD scans at low magnification from samples representing the starting condition, after tensile testing and after two conditions of R-BUT are shown in Fig. 8(a-d), respectively. These IPF maps are beneficial for understanding the deformation characteristics of the elongated grains present in the ND-RD plane of samples at different conditions. The IPF map presented in Fig. 8(a) reveals that the grains are elongated along the rolling direction and the majority of them have a crystallographic orientation of ⟨1 1 1⟩//ND. From Fig. 8(b) it is apparent that the strain imposed during tensile loading led to the formation of shear bands within the pre-existing elongated grains. Note that the shear bands generated during tensile tests are at an angle of 45° to loading direction (which is parallel to the RD). It is observed that orientation of the pre-existing grains has an influence on the direction of shear deformation occurring during tensile loading. This is confirmed by the change in orientation of the shear bands (marked by lines) activated within the grains (Fig. 8(b)). The shear deformation in R-BUT keeps changing its direction due to repeated bending and unbending resulting in the interaction of shear bands. This leads to the formation of fine grains as the level of strain imposed increases. IPF maps recorded from the R-BUT samples confirm the formation of fine grains within the prior elongated grains and along their grain boundaries, cf. Fig. 8(c) (ω = 200) and Fig. 8(d) (ω = 800). The main difference between these conditions lay in the values of penetration depth and velocity ratios (ω). A higher the penetration depth led to a decrease in the thickness of pre-existing grains and an increase in the fraction of fine grains formed (Fig. 8(c)). The formation of the fine grains is likely to be associated with a strain assisted continuous recrystallisation process due to the intense shear deformation. Fig. 8(c) and Fig. 8(d) reveal the development of a larger fraction of fine grains in the case of the R-BUT tested sample with ω = 200, as compared to the case of the sample with ω = 800. This confirms that penetration depth has major influence on the amount of shear deformation.

EBSD scans were conducted at higher magnifications on the R-BUT tested samples to confirm the underlying mechanism involved in the development of fine grains in the deforming matrix. Fig. 9(a) shows an IPF map from a higher magnification scan of the sample after R-BUT (ω = 200). The majority of the pre-existing grains covered in the scans revealed evidence of interacting shear bands during the deformation as marked by dashed lines. Also, the existence of different coloured regions within those grains confirmed the formation of fine grains having a totally different orientation than the parent grains. The IPF map from the region shown by rectangular box in Fig. 9(a), given in Fig. 9(b), confirms the existence of fine grains with an average size of less than 2.5 μm. Evidence for fine

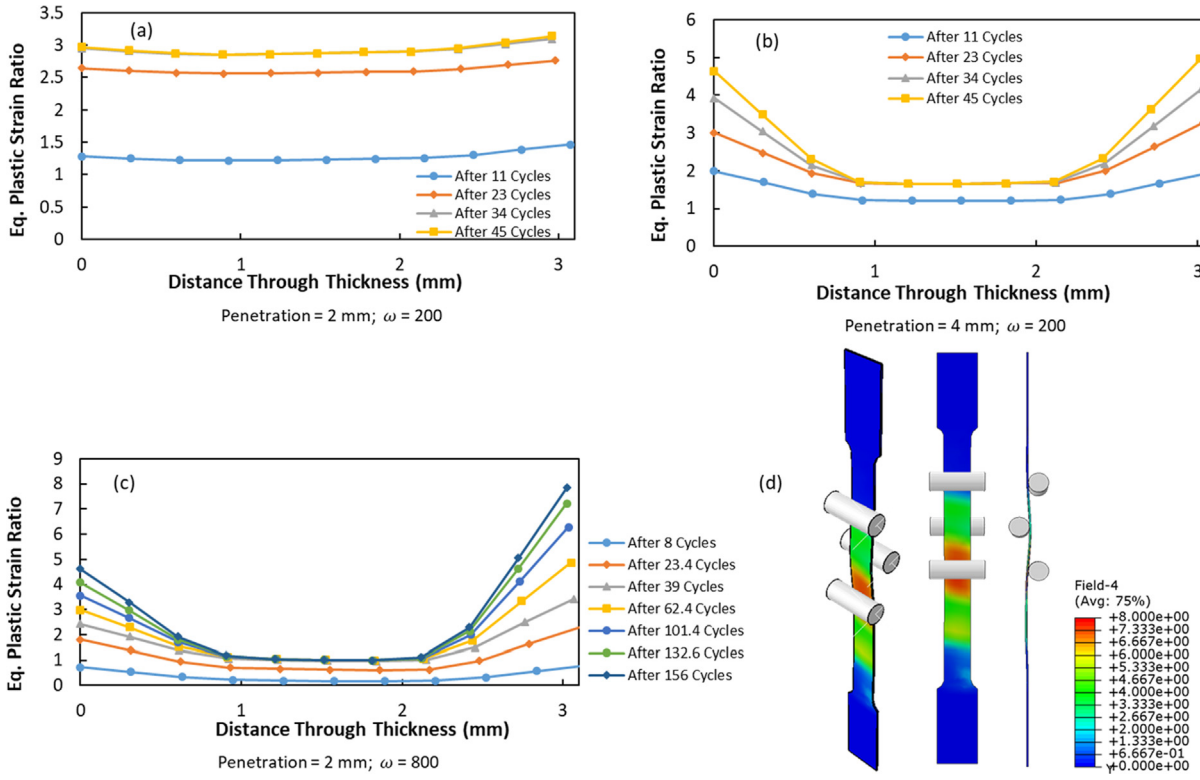

Fig. 7. (a-c) FE model predictions of the effect of R-BUT process parameters (penetration depth and velocity ratio,ω) on through thickness equivalent plastic strain ratio, (d) contour plot of equivalent strain in the sample subjected to R-BUT with penetration of 2 mm and velocity ratio of 800.

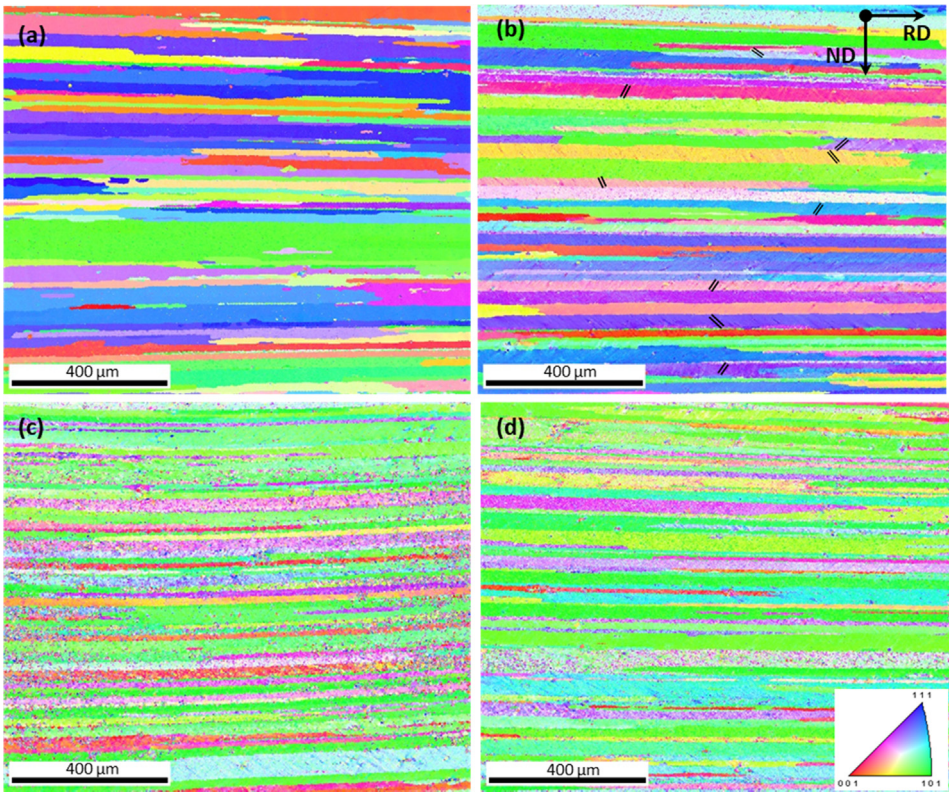

Fig. 8. ND-IPF maps from ND-RD plane of (a) starting condition, (b) after tensile test (c) after R-BUT with penetration: 4 mm and ω = 200; and (d) after R-BUT with penetration: 2 mm and ω = 800.

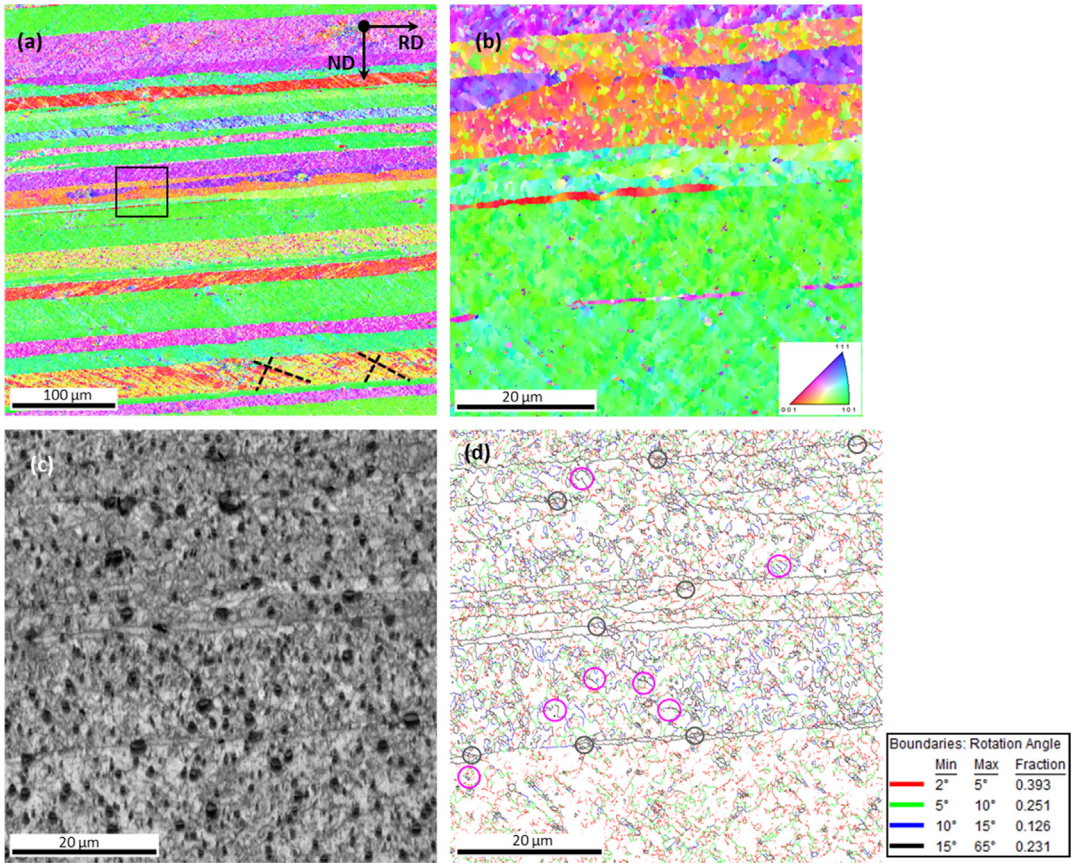

Fig. 9. (a-d) EBSD results from ND-RD plane of the R-BUT tested sample (penetration 4 mm; ω = 200) indicating the evidence for fine grains developed within the grains due to CDRX process as well as along the high angle grain boundaries of banded grains.

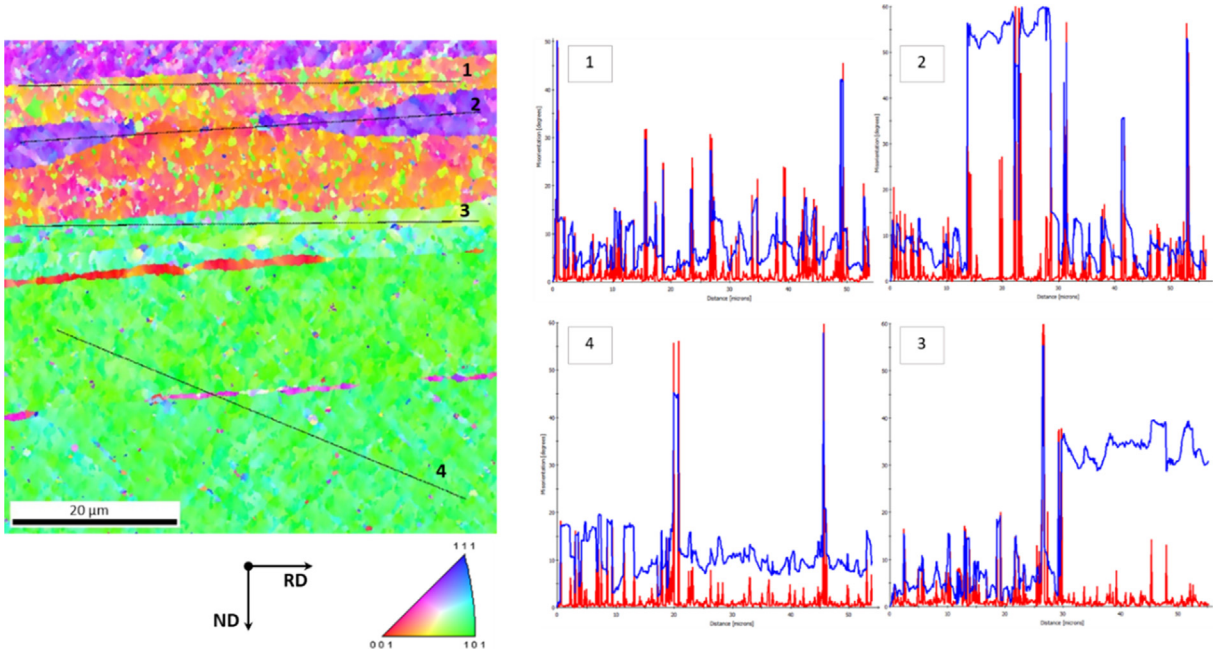

Fig. 10. Line profile analysis results from ND-RD plane of sample subjected to the R-BUT tested sample (penetration 4 mm; ω = 200) indicating the misorientation difference observed with in the pre-existing grains due to formation of fine grains with HAGB. The blue lines represent point to origin and the red lines indicate point to point misorientation angles. (For interpretation of the references to colour in this figure legend, the reader is referred to the web version of this article.)

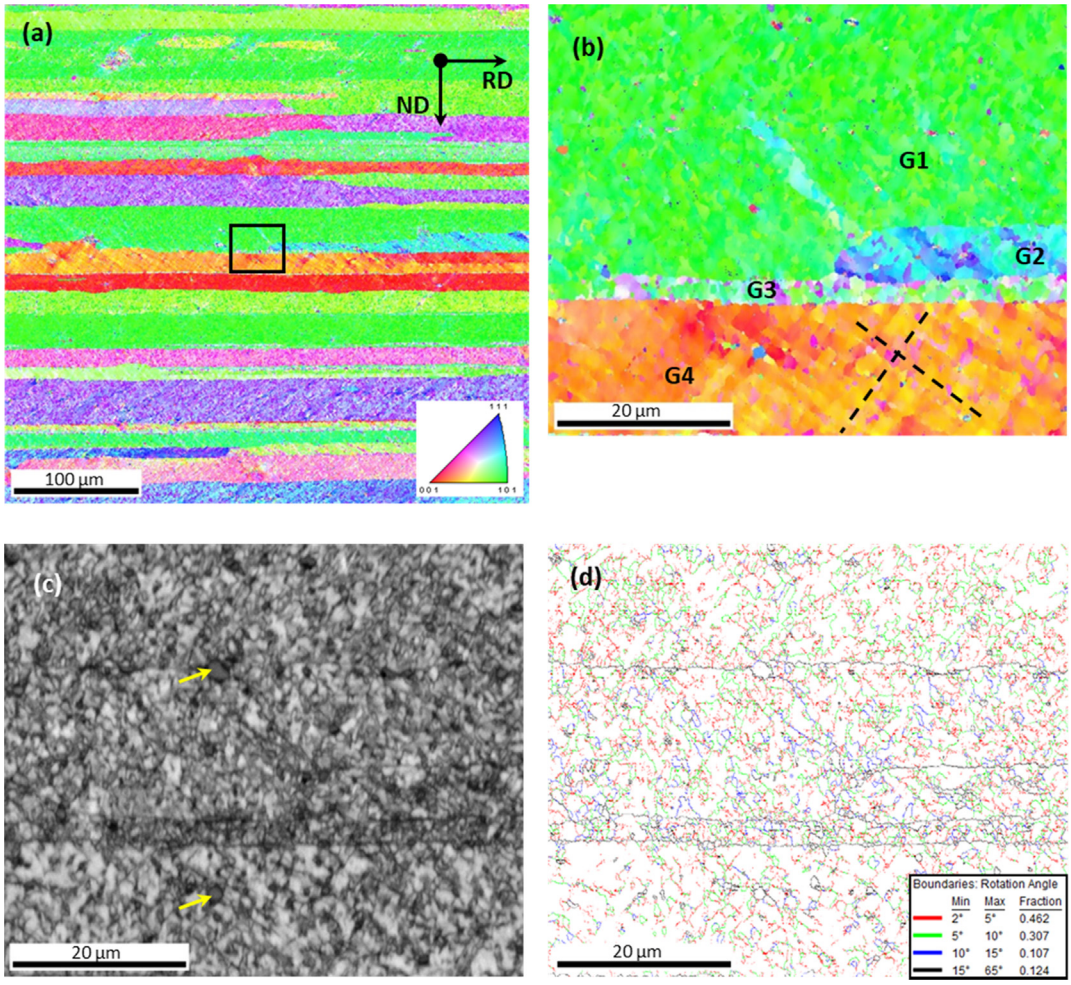

Fig. 11. (a-d) EBSD results from ND-RD plane of the R-BUT tested sample (penetration 2 mm; ω = 800) indicating the interaction of deformation bands within the elongated grains as well as fine grain formation in the matrix: (a) and (b) IPF maps; (c) Image quality map and (d) Grain boundary map.

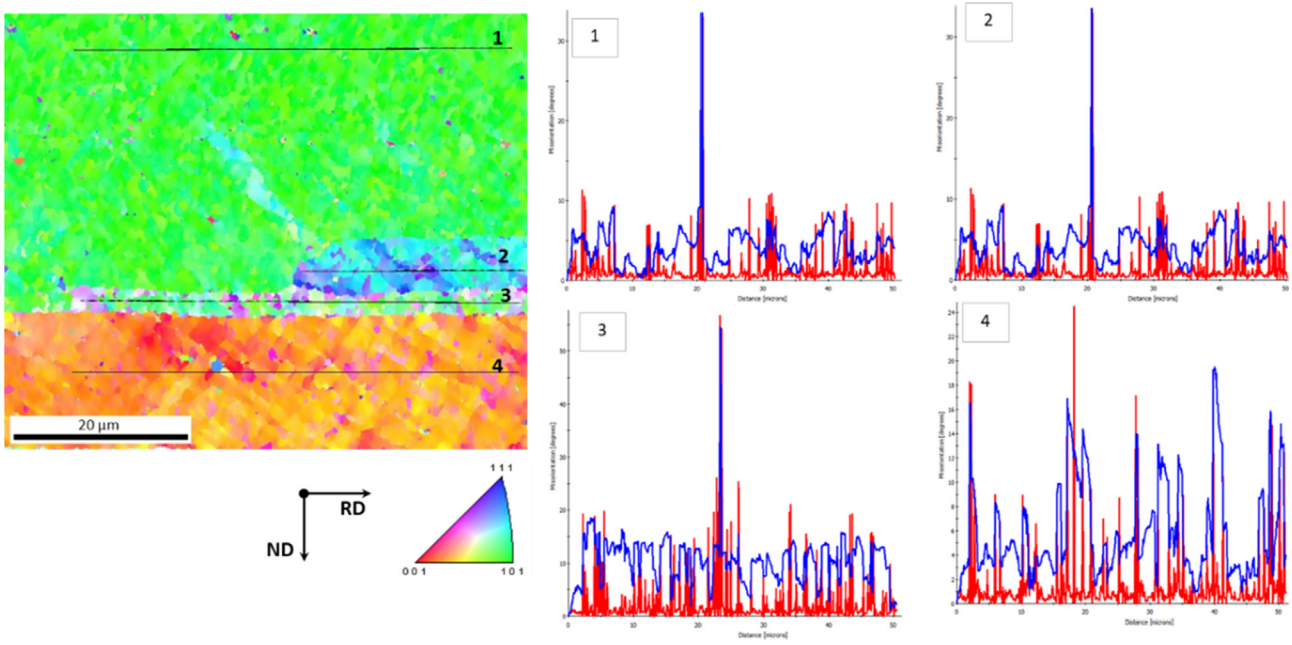

Fig. 12. Line profile analysis results from ND-RD plane of the R-BUT tested sample (penetration 2 mm; ω = 800) indicating the misorientation difference observed with in the pre-existing grains due to formation of fine grains with HAGB. The blue lines represent point to origin and the red lines indicate point to point misorientation angles. (For interpretation of the references to colour in this figure legend, the reader is referred to the web version of this article.)

grain formation is also supported by the image quality (IQ) map of the same area presented in Fig. 9(c). Dark grey features in the IQ map are the precipitate particles in the matrix. Close observation in the proximity of those particles confirmed the presence of fine grains as a result of a particle stimulated nucleation (PSN) process. The existence of these precipitates might speed up the fine grain formation by affecting localised slip activity occurring during the R-BUT process. The grain boundary character map (GB map) given in Fig. 9(d) from the same region confirmed that majority of fine grains formed are surrounded by boundaries whose misorientation angle is greater than 5° (green, blue and black). Evidence for the presence of fragments of high angle grain boundaries (misorientation angle is larger than 15°) as a product of dynamic recrystallisation during intense shear deformation is confirmed by GB map given in Fig. 9(d). Discontinuous dynamic recrystallisation (DDRX) and continuous dynamic recrystallisation (CDRX) are two types of recrystallisation process expected to operate in materials subjected to severe plastic deformation where shear is the main mode of deformation. Recent studies on SPD processed materials have claimed that CDRX is one of the dominating grain refinement mechanisms in the processed materials. CDRX is a recovery dominated process which involves progressive absorption of dislocations within grains in the vicinity of grain boundaries generating sub-grains surrounded by low angle grains boundaries (LAGB) [33,34]. Further increase in the strain imposed will lead to rotation of the sub-grains formed which ultimately transforms the LAGB in to high angle grain boundaries (HAGB). There is evidence for the formation of incomplete HAGB segments (indicated by pink circles in Fig. 9d) in the elongated grains covered by the scanned area. Formation of these incomplete segments of HAGB's are a sign for the occurrence of CDRX process during the R-BUT process. These incomplete HAGB segments are likely to have evolved from the LAGBs, due to the gradual accumulation of dislocations near to the LAGB boundaries as a result of strain imposed during the R-BUT process. Further absorption of these dislocations in the course of R-BUT will lead to the extension of these incomplete HAGB segments to form fully enclosed fine grains. Another characteristic feature associated with the CDRX process is the development of fine grains around HAGBs. The grain boundary map provided in Fig. 9(d) shows that the grain boundaries of the majority of pre-existing grains act as nucleation sites for fine grains (marked by grey circles).

Results from the line profile analysis are presented in Fig. 10 where four individual lines were used to analyse the local misorientation and orientation gradient development within the pre-existing grains of the matrix. The blue-coloured lines indicate point to origin and the red-coloured lines represent point to point misorientation angles. It is clear from the misorientation profiles that the majority of fine grains formed in the matrix as a result of CDRX process were surrounded by high angle grain boundaries (HAGB).

EBSD results from R-BUT samples of ω = 800 condition are given in Fig. 11. The IPF map given in Fig. 11(a) confirms that pre-existing grains of different orientation in the scanned area have been severely deformed. It is notable that the crystallographic orientation of each constituent grain had a major influence on the extent of plastic slip occurring as result of shear deformation during the R-BUT process. The IPF map recorded at a higher magnification from the region marked by the rectangular box in Fig. 11(a) indicates the existence of fine grains developed within the four pre-existing grains (G1, G2, G3 and G4) which had three different crystallographic orientations with respect to loading direction (Fig. 11(b)). The evidence of interacting shear bands during the R-BUT is marked by dash lines. The IQ map given in Fig. 11(c) shows the presence of precipitates (marked by yellow arrows) along with fine grains in the matrix. The fraction of fine grains formed with HAGBs were found to vary with respect to the parent grain orientation - this is shown by the GB map given in Fig. 11(d). The GB map reveals that the fraction of fine grains formed is less in the case of grain G4 as compared to other three grains namely G1, G2 and G3.

Misorientation profile analysis along lines parallel to the loading direction in all four grains are given in Fig. 12. These results confirmed that the intensity of shear deformation occurring in the pre-existing grains of the samples of ω = 800 condition is comparatively lower than the samples in the ω = 200 condition. This could be due to the reduced bending depth adopted for the R-BUT samples of the ω = 800 condition.

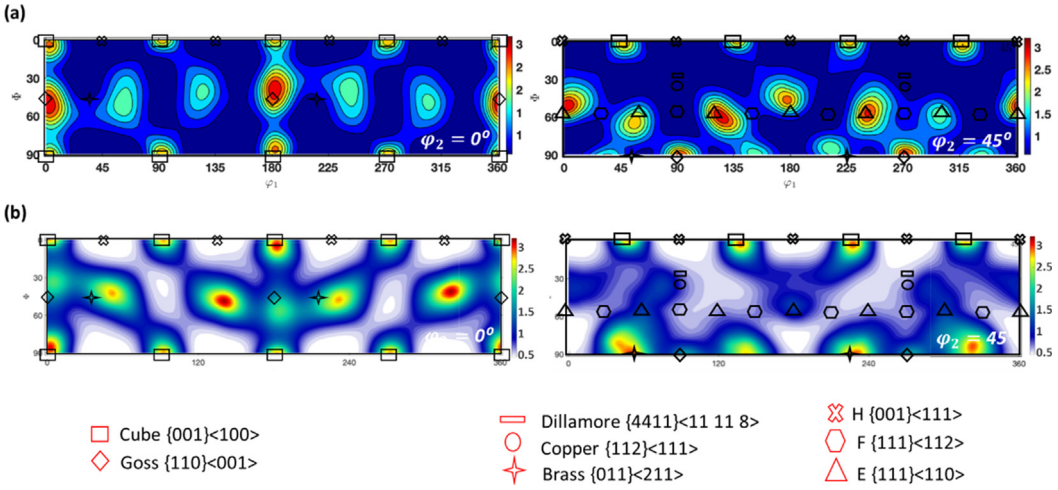

Fig. 13. Experimentally derived ODF showing the characteristics of bulk texture of (a) as-received material (b) R-BUT sample obtained by neutron diffraction.

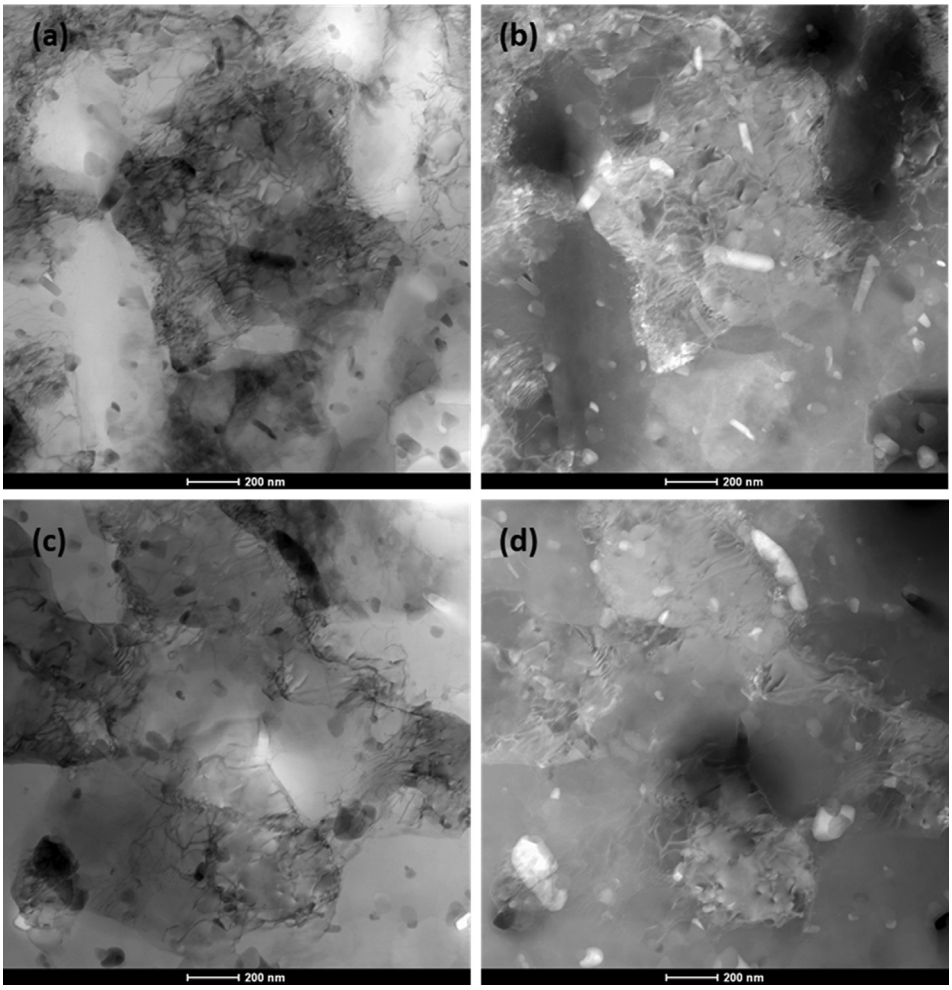

Fig. 14. (a-d) BF-HAADF pair showing the evidence for the second phase particles acting as nucleation sites for dislocations and also in the matrix of the sample after tensile testing.

3.2.2. Crystallographic texture analyses

Fig. 13 shows the ODF sections at phi$_2$ = 0° and phi$_2$ = 45° of the sample before and after the R-BUT process. The as-received sheet material has dominant cube and (1 1 1) ⟨1 1 0⟩ texture components and a weak (1 1 0) ⟨0 0 1⟩ orientation, as seen in Fig. 13(a). After processing however, (1 1 1) ⟨1 1 0⟩ has rotated towards the (0 1 1) ⟨2 1 1⟩ texture component. It is noted however that (0 0 1) ⟨1 0 0⟩ and (1 1 0) ⟨0 0 1⟩ can still be seen in the R-BUT sample

(Fig. 13(b)). In general, the (1 1 1)//ND texture is expected after universal shear plastic deformation, however, this texture usually deviates if the shear direction alters repeatedly. A similar observation has been reported for an asymmetric rolling (ASR) operation on an aluminium alloy [35]; i.e. if shear strain through ASR is applied in the same direction, (1 1 1)//ND is the main texture in the aluminium sheets whereas, this texture deviates by changing the direction of the shear strain.

3.2.3. TEM

The microstructural state of samples subjected to tensile tests are described by a set of STEM bright field (BF)/high angle annular dark field (HAADF) images from two different locations close to the fracture tip; - see Fig. 14. Note that the precipitates appear brighter in the Z-contrast HAADF images given in Fig. 14(b) and Fig. 14(d). It is clearly seen that the dislocations generated during deformation under tensile load were accumulated in the matrix in close proximity to the precipitates cf. Fig. 14(a) and Fig. 14(b). Dislocations emerging from other dislocation sources are also getting piled up against the surrounding precipitates which resulted in the formation of low angle boundaries in the deforming matrix; see Fig. 14 (c) and Fig. 14(d). Hence the precipitates present in the matrix not only acted as dislocation generation sources but also inhibited the movement of dislocations.

Due to the dynamic recovery taking place during the R-BUT process, dislocations generated in the deforming grains are expected to undergo polygonization under the influence of strain even at room temperature. The deformation mechanism activated during R-BUT is comparable to that occurring during repetitive corrugation and straightening (RCS) [12,19]. The RCS technique is also known as constrained groove pressing [36] or repeated shear deformation [37]. This is one of the top down severe plastic deformation approaches adopted to develop sheet materials with ultrafine-grains with a high fraction of HAGB. The mechanism behind the grain refinement process in the case of samples processed by RCS process includes the formation of dense dislocations walls as a result of the increase in dislocation density within the pre-existing grains. With the increase in the strain imposed through the process, these dislocation walls are converted to high-angle grain boundaries. Through the RCS process, the samples are subjected to repeated bending and un-bending under the plane-strain deformation condition without causing any change to the cross-section of the sample processed. The bending and un-bending process of sheet metal with the help of an asymmetrically grooved tool and a flat tool lead to simple shear deformation in the transverse direction. Shear strain imposed during is the shear deformation is the prime reason behind the refinement of the grains falling in the shear deformation zone (SDZ) of the processed material. It is believed that materials processed by R-BUT experience a similar deformation condition to that observed in the RCS process. The main difference is the number of cycles involving localised bending and un-bending in the processed material. This controls the amount of shear strain imposed, as well as the level of grain refinement achieved. In the case of the R-BUT process the number of cycles can be much higher than for the RCS process. This will make a significant difference in the amount of strain imposed as well as the degree of grain refinement and grain homogeneity achieved.

Supporting the above arguments, the results presented in Fig. 15 show the initial stages of grain refinement by the strain assisted recovery process; again, these were taken from a site close to the fracture tip. BF and DF pairs recorded at the different magnifications given in Fig. 15 (a-d) show the evidence for the formation sub-grain boundaries in the matrix of the R-BUT tested sample. During R-BUT, dislocation cell boundaries are initially generated within the pre-existing grains which the sub-grains subsequently forming as the amount of imposed strain increases. The BF-DF pair given in Fig. 15(e) and Fig. 15(f) shows the sub-grain formation in the region of matrix having non-deformable particles (marked by white arrows) which are less than 100 nm in diameter. Studies have confirmed that the presence of dispersoids in the size range ~ 50–100 nm in pure aluminium can accelerate grain refinement under intense shear deformation and have indicated that improved dislocation generation as well as a reduction in the slip distances have enhanced the extent of grain refinement [38]. Moreover, non-deformable particles are capable of homogenizing slip as compared to shearable particles that will result in shear localization [39]. One such shearable precipitate shearing at 3 locations (marked by a white circle) due to slip activity occurring during the deformation is shown in Fig. 15(f). It was reported that the presence of dispersoids in aluminium alloys, together with the homogenization of slip, retards the formation of intense shear bands, thus facilitating the formation of high angle grain boundaries [40,41].

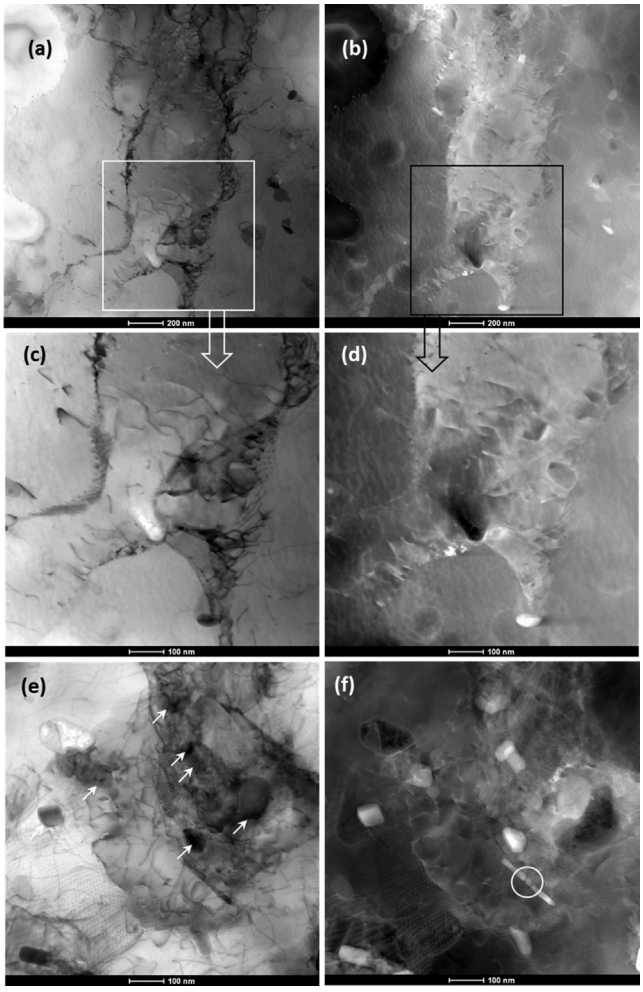

Fig. 15. (a-f) BF-DF pairs showing the formation of sub-grain boundaries within the pre-existing grains of the R-BUT tested samples as result of dynamic recovery.

BF-DF pairs from different locations of R-BUT tested samples in Fig. 16 show evidence for fragmentation of second phase particles during processing. Dotted ellipses are used to mark the shearing precipitates due to the interaction with deformation bands which occurred during the R-BUT process. The majority of the precipitate laths are breaking at more than one location. In addition to that it appeared that fragments of those precipitates were partially spheroidized. Evidence for fragmented pieces of precipitates undergoing

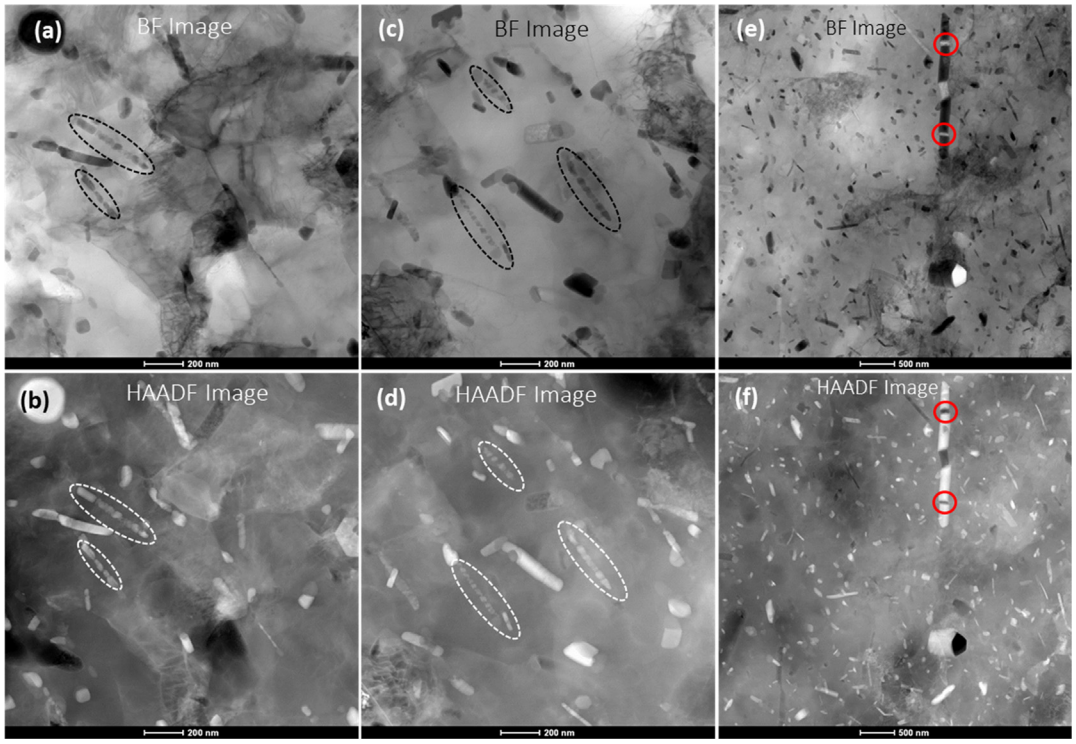

Fig. 16. (a-f) BF-HAADF pairs recorded from the samples after R-BUT confirms the fragmentation of precipitate laths as well as strain induced spheroidization of fragments.

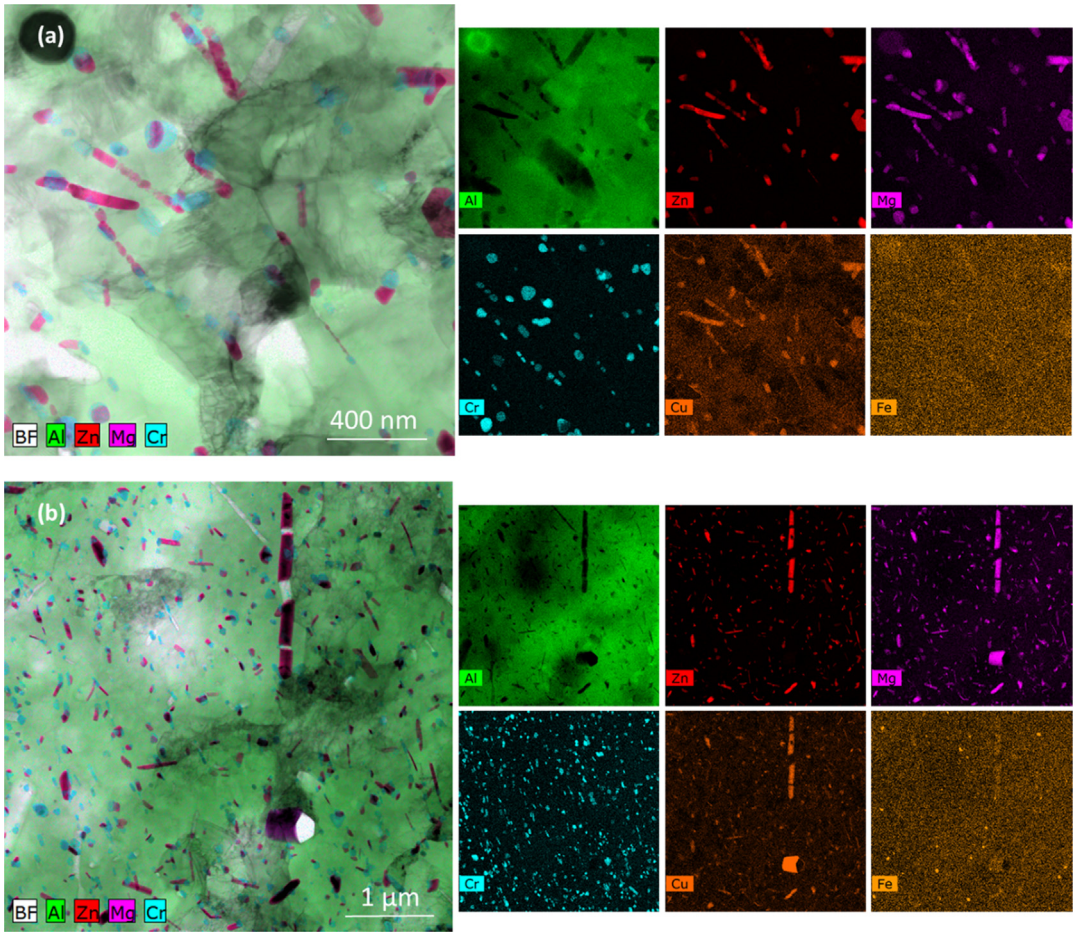

Fig. 17. Composite maps of Al, Zn, Mg, Cr overlapped on STEM BF images, and individual elemental maps of Al, Zn, Mg, Fe, Cu and Cr. (a) the scanned area presented in Fig. 16a and (b) the scanned area presented in Fig. 16e.

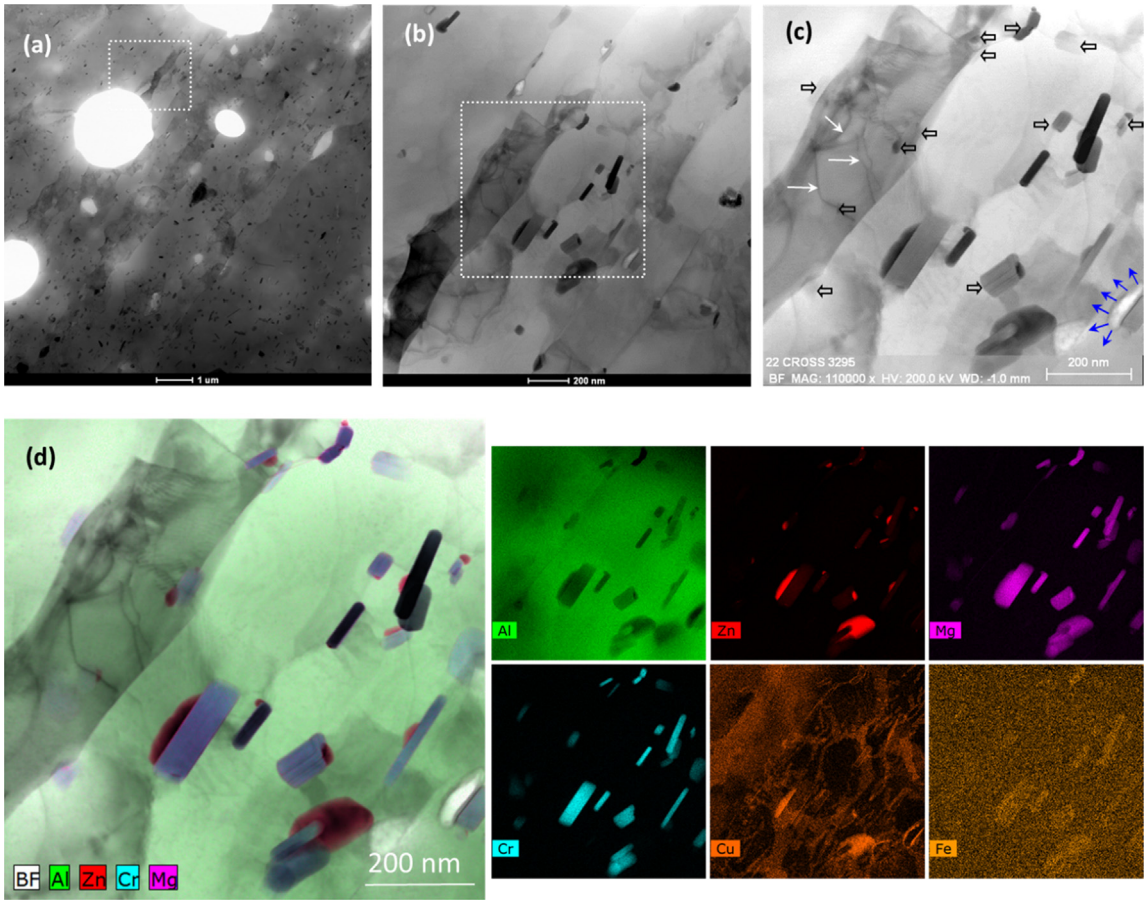

Fig. 18. (a-c) Bright field micrographs recorded at different magnification shows the sub-grains formed within the grains of sample after R-BUT, (d) composite map of Al, Zn, Mg, Cr overlapped on STEM BF image, and individual elemental maps of Al, Zn, Mg, Fe, Cu and Cr.

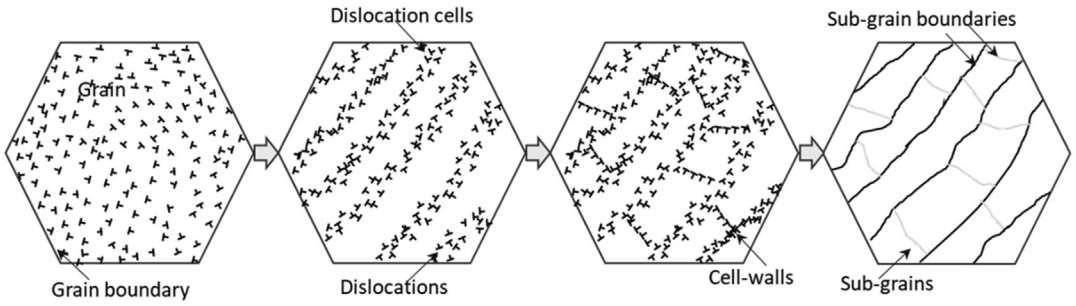

Fig. 19. Schematic illustrating the formation of elongated sub-grains as well as their sub-division due to creation of transverse boundaries as an outcome of dynamic recovery.

strain assisted spheroidization is seen clearly with in the dotted ellipses shown in Fig. 16(a-d). Fig. 16(a) and Fig. 16(b) show that the fragmented precipitates distributed in the matrix tend to provide preferential sites for dislocations to develop more deformation induced boundaries which would offer obstacles to the dislocation movement, thereby resulting in an overall finer structure. The BF-DF pairs recorded at the lower magnification illustrate the distribution of fragments of second phase particles in the matrix (Fig. 16(e) and Fig. 16(f)). Moreover, this pair of micrographs shows the presence of more weakly misoriented and diffuse boundaries in the matrix. Fine second phase particles distributed in the matrix cause an increase in the rate of dislocation generation by encouraging the formation of Orowan and prismatic loops during low strain deformation [42,43]. The dislocation density will be higher closer to those particles and that will lead to nucleation of very fine grains in their proximity. Thus, the presence of fine particles will increase the degree of grain refinement in addition to the DRX process occurring in the deforming matrix to form fine grains [44].

In order to determine the composition of the precipitates undergoing fragmentation or shearing the HAADF imaging with the STEM mode was adopted. Results from EDS analysis of regions covered by the BF-DF pairs given in Fig. 16(a-b) and Fig. 16(e-f) are presented in Fig. 17(a) and Fig. 17(b), respectively. Composition maps of elements like Al, Zn Mg, Cu, Cr and Fe are also presented. It is confirmed from the EDS results given in Fig. 17 that the rod like precipitates (called as η) were those fragmented due to slip activity occurring within the grains. The main constituent ele-

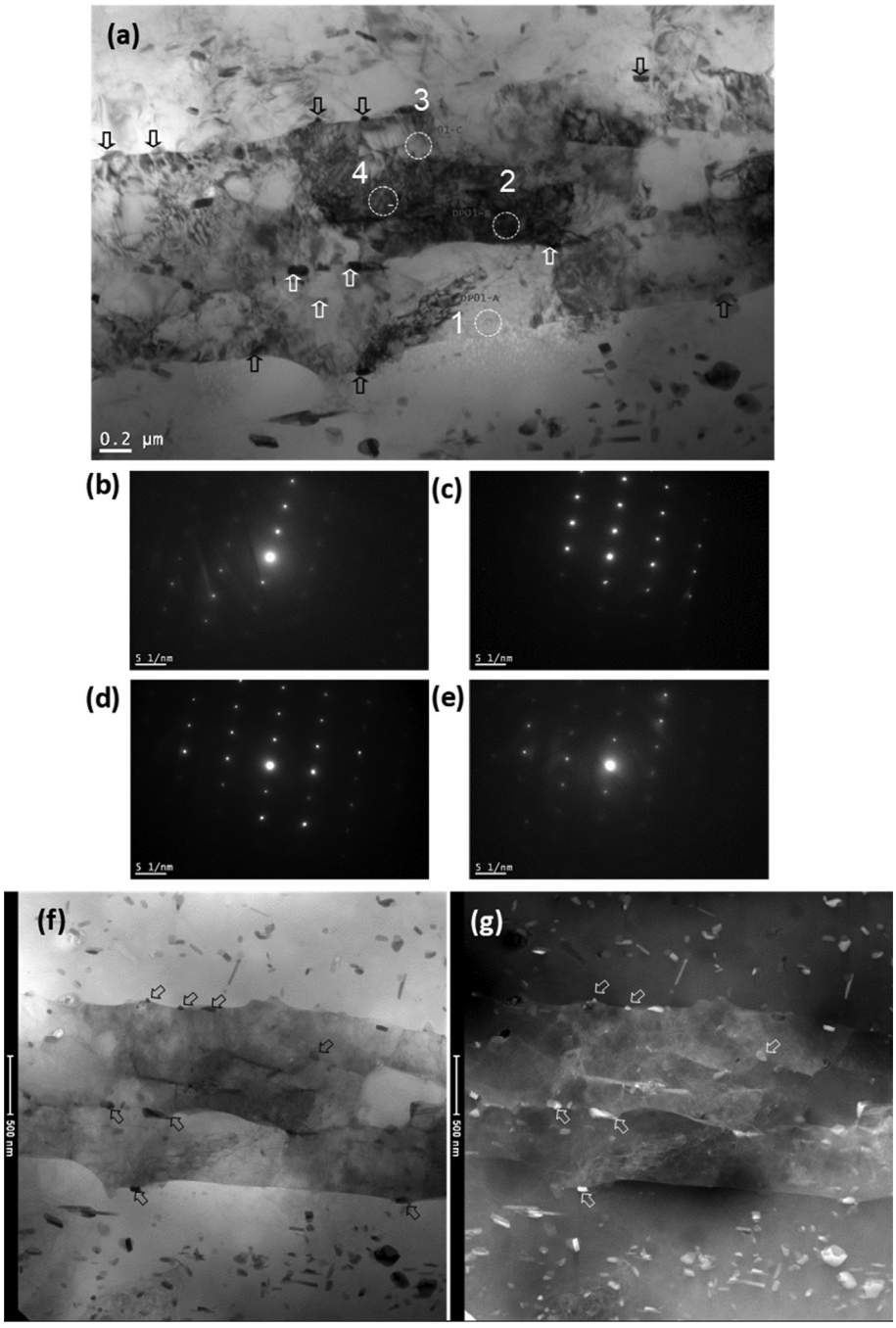

Fig. 20. (a) BF micrograph showing the sub-grains formed in the matrix of samples after R-BUT. (b)-(e) SADP patterns from sub grains 1, 2, 3 and 4, respectively (marked by dotted circles); Open arrows indicate the precipitates pinning the grain boundaries. (f)-(g) BF-DF pair from the region at different tilt conditions showing the evidence for precipitates pinning the boundaries of sub-grains formed.

ments of those precipitates are Zn, Mg, and Cu. Due to the presence of the heavier alloying elements like Zn, the rod like precipitates observed in HAADF images given in Fig. 16 appeared bright due to atomic number contrast.

Evidence for formation of elongated grains in the direction of shear deformation that occurred in the matrix is shown in Fig. 18 (a). The BF image shown in Fig. 18(b) is the magnified region marked by the rectangular box on Fig. 18(a). It is clearly seen that many precipitates are pinning the boundaries of the elongated grains. At very high strain levels, the microstructure will undergo further refinement by progressive breaking up of these elongated grains into sub-grains having a lower aspect ratio; this is observed in Fig. 18 (b). Fig. 18(c) shows that these elongated grains are generally found to subdivide by specific transverse boundaries. These transverse boundaries will undergo a high rate of misorientation change as the extent of strain enforced in the deforming matrix increases. The breakup of the elongated grains may be accelerated by heterogeneities caused by second phase particles in the plastic flow, as indicated in Fig. 18(c). Similar observations are reported in TEM analysis made on severely deformed aluminium alloys [45]. EDS results given in Fig. 18(d) help to identify the elemental distribution in the deforming matrix as well as in the different types of precipitates in the matrix shown in Fig. 18(c). A grain refinement model has been proposed to explain the formation of elongated subgrains by dynamic recovery as well as for sub-division of such elongated grains by formation of transverse boundaries; see Fig. 19.

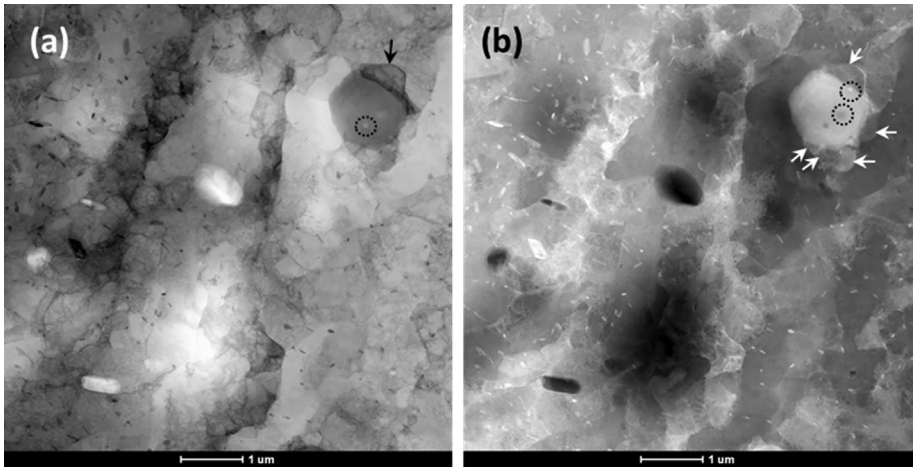

Fig. 21. (a-b) BF-DF pair recorded from R-BUT tested sample indicating the presence of fine grains with dislocations formation in the matrix having distribution fine precipitates and evidence for the formation of fine grains around the second phase particle due to particle stimulated nucleation process.

Fig. 19(a) shows the random distribution of dislocations generated during deformation due to activation of dislocation sources within the grains. An increase in the strain imposed leads to dynamic recovery which results in the formation of elongated dislocation cells as shown in Fig. 19(b) and these cells transform into sub-grain boundaries. As dislocations are generated, further straining of the material leads to formation of random boundaries in the transverse direction. As a result, the elongated sub-grains formed are divided into equiaxed sub-grains as illustrated in Fig. 19(d). The distance of separation between these elongated sub-grain boundaries will decide the size of the sub-grains formed within the pre-existing grains. Some studies on severe plastic deformation routes to generate fine grains have claimed that grain boundary diffusion assisted reorganization process plays a key role in the formation of equiaxed ultrafine grains from elongated sub-grain boundaries [46]. By progressing the process, the level of imposed shear strain on the material increases leading to an increase the misorientation across sub-grain boundaries (low-angle grain boundaries (LAGB)). These LAGB are eventually transformed into boundaries with high misorientation (HAGB) [47]. The presence of precipitates in the matrix may facilitate the above mentioned steps of the grain refinement process, which is evident in the bight field micrographs shown in Fig. 18.

The particle pinning of boundaries leading to ultrafine grain range is clear from the BF micrograph shown in Fig. 20(a). This can be deduced from the fact that all the fine grains in the micrograph are in the sub-micrometre range. SADP patterns shown in Fig. 20(b-e) that were recorded using the smallest possible aperture on some of the fine grains (marked as 1, 2, 3 & 4) in Fig. 20 (a) confirm the presence of fine grains in the size range 200–400 nm. Those particles pinning the boundaries (indicated by open arrow) may be a second phase precipitated in the matrix or alternatively could be the fragments of precipitates sheared during the deformation which occurred during R-BUT. The BF-DF pair recorded from the region at a different tilt condition clearly shows the evidence for precipitates pinning the grain boundaries of sub-grains formed (Fig. 20(f) and Fig. 20(g)). Presence of such precipitates along the sub-grain boundaries may also help to stabilize the grain size via the Zener drag effect. Also, the presence of such precipitates at grain boundaries will lower their interface and boundary energy. Force must be exerted in order to move the boundary past a particle. This is a function of the particle size and the energy of the migrating boundary [48]. Precipitates which are pinning at the grain boundaries can be coarsened quickly as a result of accelerated diffusion of alloying elements needed for their growth. This may lead to more efficient pinning of the grain boundaries causing grain growth to be retarded when the material is exposed to elevated temperatures. Second phase particles present during the deformation of the materials often use dislocation substructure as sites to nucleate and grow. When aluminium alloys with non-deformable particles are subjected to severe plastic deformation, an incompatibility may develop between them and deforming matrix. This can result from the activation of different slip systems around the particle during plastic deformation. The surrounding matrix may rotate to bring down the incompatibility with the non-deforming particles. The localized zones developed as a result of this process are called particle deformation zones (PDZ) [49,50]. The size of the PDZs formed depends on the level of strain imposed and the size of the non-deformable particles. Dislocations are generated at the interface between the particle and matrix during the process of the PDZ formation and this leads to an increase in dislocation density close to those particles [51,52].

Localization of strain incompatibility between the deforming matrix and non-deformable second phase particles is also expected to develop in the aluminium alloy tested during the R-BUT process. A high density of dislocations generated during an SPD process like R-BUT accumulates in the surrounding area of the particles to adjust such strain incompatibility [53]. Localised differences in the effective strain imposed during the process lead to differences in the dislocation densities generated in the particle free zones of the matrix and at sites adjacent to the particles. Number of dislocations getting stored close to the particle are expected to be significantly high as compared to the particle free zones in the matrix. It was reported that PDZ's can be act as sites for particle stimulated nucleation (PSN) for recrystallisation of new dislocation free fine grains [54–58,51] in the case of aluminium alloys during deformation at room temperature. The PDZs act as a driving force for nucleation of crystallites in and around the second phase particles which remain non-deformable during the deformation. This results in formation of recrystallization nuclei in the deformation zones [59]. If several crystallites nucleate at a particle, then the efficiency of PSN is claimed to be greater than one [60]. It was shown that multiple new crystallites are expected to nucleate only when the second phase particles formed in the matrix in the size range of 5–10 μm [61]. But the size range of the non-deformable particle shown in the BF-DF pair presented in Fig. 21 is around 1 μm and multiple active nucleation sites were noted.

Hence, the complex stress conditions generated during the R-BUT would tend to support multiple nucleation around particles of the type shown. It is also expected that there will be a mild

increase in temperature of the matrix near such non-deformable particles during severe plastic deformation. Normally, continuous dynamic recrystallization is expected to happen when materials are subjected to plastic deformation at higher temperatures. However, due to the severity of the deformation occurring during the R-BUT process at ambient temperature conditions were favourable for recrystallization to occur dynamically in the areas close the hard second phase particles; see Fig. 21. Therefore, continuous dynamic recrystallization is suggested to be the main mechanism behind the grain refinement process. Possibilities for developing ultrafine-grains in the case of Al alloys with significant volume fractions of second-phase particles after severe plastic deformation processes were reported in [41,62,63]. Similar dynamic recovery and recrystallization behaviour around precipitates has been reported in the case of Al-Li alloy [64] and Al-Mg alloy [65] after severe plastic deformation conducted at ambient temperature.

4. Conclusions

This work aimed to investigate the feasibility of the R-BUT process for developing an ultrafine-grained AA-7075 alloy through repetitive bending and unbending under tension. The notable findings of this study are listed below:

- The influence of two important R-BUT process parameters; namely the velocity ratio, and the bending level, on the formability of the alloy is presented. It is shown that by optimizing the parameters, a 220% increase in uniform elongation, as well as an 80% reduction in the maximum required force compared to a standard tensile test, can be achieved.
- FE analyses confirmed that the R-BUT tested sample underwent shear deformation which played a critical role for grain refinement in the processed samples.
- Neutron diffraction analyses indicated that an initial gamma fibre texture deviated towards a brass texture after the R-BUT process. This was due to the repetitive change in the direction of shear deformation experienced by the gauge sections of the samples as they underwent the R-BUT process.
- A detailed microstructural analysis using TEM confirmed that ultrafine-grains were formed in AA-7075 alloy sheets using R-BUT at room temperature. The presence of fine precipitates in the matrix increased the grain refinement process through a particle stimulated nucleation process.
- TEM results revealed shearing of precipitate laths due to the intense shear deformation occurring in the samples. In addition to that, evidence for spheroidization of the fragmented pieces of precipitate laths in the deforming matrix is also reported.
- EBSD investigations on the R-BUT processed samples confirmed that continuous dynamic recrystallisation (CDRX) is the major mechanism behind the formation of fine grains in the matrix of AA-7075 alloy.

The work suggests that R-BUT could be a top-down SPD approach to fabricate sheet metals with ultrafine-grains. This process can be up-scaled to produce large-size sheet metal blanks with ultrafine-grains at industrial scale by having multiple rollers arrangements.

5. Data availability

The raw and processed data required to regenerate these findings will be shared with interested parties upon reasonable request.

Declaration of Competing Interest

The authors declare that they have no known competing financial interests or personal relationships that could have appeared to influence the work reported in this paper.

Acknowledgments

The authors would like to acknowledge the support provided by the Advanced Forming Research Centre (AFRC), University of Strathclyde (under the project AFRC_CATP_1186).

References

[1] S. Suwas, S. Mondal, Texture Evolution in Severe Plastic Deformation Processes, Mater. Trans. (2019). pp. MF201933.
[2] Y. Iwahashi, Z. Horita, M. Nemoto, J. Wang, T.G. Langdon, Principle of equal-channel angular pressing for the processing of ultra-fine grained materials, Scripta materialia 35 (2) (1996).
[3] R.Z. Valiev, T.G. Langdon, Principles of equal-channel angular pressing as a processing tool for grain refinement, Prog. Mater Sci. 51 (7) (2006) 881–981.
[4] A. Rosochowski, L. Olejnik, M.W. Richert, Double-billet incremental ECAP, in: Materials Science Forum, vol. 584, Trans Tech Publ, 2008, pp. 139–144.
[5] M.R. Salamati, M.J. Qarni, S. Tamimi, A. Rosochowski, Effect of channel angle on the material flow, hardness distribution and process forces during incremental ECAP of Al-1050 billets, in: AIP Conference Proceedings, vol. 1769, no. 1: AIP Publishing LLC, 2016, pp. 090004.
[6] S. Naghdy, H. Pirgazi, P. Verleysen, R. Petrov, L. Kestens, Morphological and crystallographic anisotropy of severely deformed commercially pure aluminium by three-dimensional electron backscatter diffraction, J. Appl. Crystallogr. 50 (5) (2017) 1512–1523.
[7] K. Edalati, Z. Horita, A review on high-pressure torsion (HPT) from 1935 to 1988, Mater. Sci. Eng., A 652 (2016) 325–352.
[8] H. Pirgazi, A. Akbarzadeh, Characterization of nanostructured aluminum sheets processed by accumulative roll bonding, Int. J. Mod Phys B 22 (18n19) (2008) 2840–2847.
[9] S. Tamimi, M. Ketabchi, N. Parvin, M. Sanjari, A. Lopes, Accumulative Roll Bonding of pure copper and IF steel, Int. J. Metals 2014 (2014).
[10] R. Kapoor, A. Sarkar, R. Yogi, S. Shekhawat, I. Samajdar, J. Chakravartty, Softening of Al during multi-axial forging in a channel die, Mater. Sci. Eng., A 560 (2013) 404–412.
[11] Q. Chen, D. Shu, C. Hu, Z. Zhao, B. Yuan, Grain refinement in an as-cast AZ61 magnesium alloy processed by multi-axial forging under the multitemperature processing procedure, Mater. Sci. Eng., A 541 (2012) 98–104.
[12] J. Huang, Y. Zhu, H. Jiang, T. Lowe, Microstructures and dislocation configurations in nanostructured Cu processed by repetitive corrugation and straightening, Acta Mater. 49 (9) (2001) 1497–1505.
[13] J. Huang, Y.T. Zhu, D.J. Alexander, X. Liao, T.C. Lowe, R.J. Asaro, Development of repetitive corrugation and straightening, Mater. Sci. Eng., A 371 (1–2) (2004) 35–39.
[14] Y. Beygelzimer, V. Varyukhin, S. Synkov, D. Orlov, Useful properties of twist extrusion, Mater. Sci. Eng., A 503 (1–2) (2009) 14–17.
[15] V. Varyukhin, Y. Beygelzimer, S. Synkov, D. Orlov, Application of twist extrusion, in: Materials Science Forum, vol. 503: Trans Tech Publ, 2006, pp. 335–340.
[16] S.S. Kumar, T. Raghu, Structural and mechanical behaviour of severe plastically deformed high purity aluminium sheets processed by constrained groove pressing technique, Mater. Des. 57 (2014) 114–120.
[17] F. Khodabakhshi, M. Kazeminezhad, The effect of constrained groove pressing on grain size, dislocation density and electrical resistivity of low carbon steel, Mater. Des. 32 (6) (2011) 3280–3286.
[18] S. Lee, Y. Saito, N. Tsuji, H. Utsunomiya, T. Sakai, Role of shear strain in ultragrain refinement by accumulative roll-bonding (ARB) process, Scr. Mater. 46 (4) (2002) 281–285.
[19] N. Thangapandian, S.B. Prabu, K. Padmanabhan, Effects of die profile on grain refinement in Al–Mg alloy processed by repetitive corrugation and straightening, Mater. Sci. Eng., A 649 (2016) 229–238.
[20] S. Tamimi, G. Sivaswamy, M.A. Siddiq, A. Leacock, P. Blackwell, Mechanical response and microstructure evolution of commercially pure titanium subjected to repetitive bending under tension, Mater. Des. (2020) 108814.
[21] J. Benedyk, N. Parikh, D. Stawarz, A method for increasing elongation values for ferrous and nonferrous sheet metals(Ferrous and nonferrous sheet metals neck formation prevention for increasing elongation in tensile tests, using continuous plastic bending method), J. Mater. 6 (1971) 16–29.
[22] W. Emmens, A.H. van den Boogaard, Incremental forming by continuous bending under tension—an experimental investigation, J. Mater. Process. Technol. 209 (14) (2009) 5456–5463.
[23] T.J. Roemer, B.L. Kinsey, Y.P. Korkolis, Design of a continuous-bending-under-tension machine and initial experiments on AL-6022-T4, in: International Manufacturing Science and Engineering Conference, vol. 56826: American Society of Mechanical Engineers, 2015, pp. V001T02A099.

[24] T. Barrett, B. Kinsey, M. Knezevic, Y. Korkolis, Numerical and experimental investigation of formability enhancement during continuous-bending-under-tension (CBT) of AA6022-T4, Procedia Eng. 207 (2017) 1940–1945.
[25] M. Zecevic, T.J. Roemer, M. Knezevic, Y.P. Korkolis, B.L. Kinsey, Residual ductility and microstructural evolution in continuous-bending-under-tension of AA-6022-T4, Materials 9 (3) (2016) 130.
[26] C.M. Poulin, S.C. Vogel, Y.P. Korkolis, B.L. Kinsey, M. Knezevic, Experimental studies into the role of cyclic bending during stretching of dual-phase steel sheets, Int. J. Mater. Form. (2020) 1–16.
[27] W. Kockelmann, L. Chapon, P. Radaelli, Neutron texture analysis on GEM at ISIS, Physica B 385 (2006) 639–643.
[28] H. Wenk, L. Lutterotti, S. Vogel, Rietveld texture analysis from TOF neutron diffraction data, Powder Diffr. 25 (3) (2010) 283–296.
[29] R. Hielscher, H. Schaeben, A novel pole figure inversion method: specification of the MTEX algorithm, J. Appl. Crystallogr. 41 (6) (2008) 1024–1037.
[30] S. Tamimi, A. Andrade-Campos, J. Pinho-da-Cruz, Modelling the Portevin-Le Chatelier effects in aluminium alloys: a review, J. Mech. Behav. Mater. 24 (3–4) (2015) 67–78.
[31] D. Thevenet, M. Mliha-Touati, A. Zeghloul, The effect of precipitation on the Portevin-Le Chatelier effect in an Al–Zn–Mg–Cu alloy, Mater. Sci. Eng., A 266 (1–2) (1999) 175–182.
[32] A. Hadoush, A.H. van den Boogaard, W. Emmens, A numerical investigation of the continuous bending under tension test, J. Mater. Process. Technol. 211 (12) (2011) 1948–1956.
[33] M.J. Qarni, G. Sivaswamy, A. Rosochowski, S. Boczkal, Effect of incremental equal channel angular pressing (I-ECAP) on the microstructural characteristics and mechanical behaviour of commercially pure titanium, Mater. Des. 122 (2017) 385–402.
[34] M. Salamati, S. Tamimi, S. Moturu, G. Sivaswamy, M. Qarni, A. Rosochowski, Microstructure and mechanical properties of Al-1050 during incremental ECAP, IOP Conference Series: Materials Science and Engineering vol. 194 (1) (2017).
[35] S. Tamimi, J.P. Correia, A.B. Lopes, S. Ahzi, F. Barlat, J.J. Gracio, Asymmetric rolling of thin AA-5182 sheets: Modelling and experiments, Mater. Sci. Eng., A 603 (2014) 150–159.
[36] D.H. Shin, J.-J. Park, Y.-S. Kim, K.-T. Park, Constrained groove pressing and its application to grain refinement of aluminum, Mater. Sci. Eng., A 328 (1–2) (2002) 98–103.
[37] M.Y. Huh, H. Kim, O. Engler, Evolution of texture and microstructure during repeated shear deformation in aluminum 1100 alloy sheets, in: Materials Science Forum, vol. 396, no. 1: Trans Tech Publications, 2002, pp. 447–452.
[38] C. Barlow, N. Hansen, Y. Liu, Fine scale structures from deformation of aluminium containing small alumina particles, Acta Mater. 50 (1) (2002) 171–182.
[39] J. Martin, Precipitation Hardening, pp. 89Butterworth, ed: Heinemann, Oxford, 1998.
[40] M. Berta, P.B. Prangnell, The effect of dispersoids and processing variables on grain refinement of aluminium alloys deformed by ECAE, in: Solid State Phenomena, vol. 114: Trans Tech Publ, 2006, pp. 151–158.
[41] P. Apps, M. Berta, P. Prangnell, The effect of dispersoids on the grain refinement mechanisms during deformation of aluminium alloys to ultra-high strains, Acta Mater. 53 (2) (2005) 499–511.
[42] M. Ashby, The deformation of plastically non-homogeneous materials, Philos. Magazine: J. Theor. Exp. Appl. Phys. 21 (170) (1970) 399–424.
[43] P. Hirsch, F. Humphreys, Physics of Strength and Plasticity, MIT Press, Cambridge, 1969.
[44] F. Humphreys, P. Hirsch, Work-hardening and recovery of dispersion hardened alloys, Phil. Mag. 34 (3) (1976) 373–390.
[45] F. Humphreys, M. Ardakani, The deformation of particle-containing aluminium single crystals, Acta Metall. Mater. 42 (3) (1994) 749–761.
[46] A. Mishra, V. Richard, F. Gregori, R. Asaro, M. Meyers, Microstructural evolution in copper processed by severe plastic deformation, Mater. Sci. Eng., A 410 (2005) 290–298.
[47] F. Humphrey, P.A. Prangnell, R. Nonmn, A. Ghollnla, C.J. Harris, Philos. Trans. R. Soc. (London) A 357 (1999) 1663–1681.
[48] F. Humphreys, M. Hatherly, Grain growth and related annealing phenomena, ed: Eleselvier Science Ltd., Oxford, UK, 1995.
[49] R. Doherty et al., Current issues in recrystallization: a review, Mater. Sci. Eng., A 238 (2) (1997) 219–274.
[50] M. Ashby, Work hardening of dispersion-hardened crystals, Phil. Mag. 14 (132) (1966) 1157–1178.
[51] F. Humpreys, M. Hatherly, Recrystallization and Related Annealing Phenomena, Elsevier, Kidlington, 2004.
[52] S. Tangen, K. Sjølstad, T. Furu, E. Nes, Effect of concurrent precipitation on recrystallization and evolution of the P-texture component in a commercial Al-Mn alloy, Metall. Mater. Trans. A 41 (11) (2010) 2970–2983.
[53] H. Gleiter, B. Chalmers, Prog. Mater Sci. (1989).
[54] F. Humphreys, Local lattice rotations at second phase particles in deformed metals, Acta Metall. 27 (12) (1979) 1801–1814.
[55] O. Engler, X. Kong, K. Lücke, Development of microstructure and texture during rolling of single-phase and two-phase cube-oriented Al-Cu single crystals, Scripta materialia 41 (5) (1999).
[56] F. Humphreys, P. Kalu, The plasticity of particle-containing polycrystals, Acta Metall. Mater. 38 (6) (1990) 917–930.
[57] B. Radhakrishnan, G. Sarma, H. Weiland, P. Baggethun, Simulations of deformation and recrystallization of single crystals of aluminium containing hard particles, Modell. Simul. Mater. Sci. Eng. 8 (5) (2000) 737.
[58] J. Humphreys, P. Bate, Gradient plasticity and deformation structures around inclusions, Scr. Mater. 48 (2) (2003) 173–178.
[59] F. Humphreys, The nucleation of recrystallization at second phase particles in deformed aluminium, Acta Metall. 25 (11) (1977) 1323–1344.
[60] X. Lei et al., Particle stimulated nucleation revisited in three dimensions: a laboratory-based multimodal X-ray tomography investigation, Mater. Res. Lett. 9 (1) (2021) 65–70.
[61] J.A. Wert, N. Paton, C. Hamilton, M. Mahoney, Grain refinement in 7075 aluminum by thermomechanical processing, Metall. Trans. A 12 (7) (1981) 1267–1276.
[62] P. Apps, J.R. Bowen, P. Prangnell, The effect of coarse second-phase particles on the rate of grain refinement during severe deformation processing, Acta Mater. 51 (10) (2003) 2811–2822.
[63] Y. Huang, Y. Liu, P. Wambua, Formation of ultrafine scale structures in aluminium containing small amounts of particles by conventional rolling deformation, J. Mater. Sci. 36 (19) (2001) 4711–4717.
[64] S. Giribaskar, R. Prasad, Dynamic Recrystallization in Al-Li Based Alloy during Equal Channel Angular Extrusion, in: Materials Science Forum, vol. 715, Trans Tech Publ, 2012, pp. 286–291.
[65] S. Giribaskar, R. Prasad, J. Ramkumar, TEM studies on recovery and recrystallisation in Equal Channel Angular Extrusion processed Al-3% Mg alloy, Trans. Indian Inst. Met. 61 (2–3) (2008) 173–176.